2017

The effects of CTDSP1 on topoI degradation and cellular resistance to topoI inhibitors chemotherapy treatment

BOSTON UNIVERSITY

SCHOOL OF MEDICINE

Thesis

THE EFFECTS OF CTDSP1 ON TOPOI DEGRADATION AND CELLULAR RESISTANCE TO TOPOI INHIBITORS CHEMOTHERAPY TREATMENT

by

EMMA SWAYZE

B.S., Boston College, 2015

Submitted in partial fulfillment of the

requirements for the degree of

Master of Science

2017

Approved by

First Reader

Ajit Bharti, Ph.D
Assistant Professor of Medicine
Section of Hematology & Oncology

Second Reader

Shuaiying Cui, Ph.D
Assistant Professor of Medicine
Section of Hematology & Oncology

DEDICATION

I would like to dedicate this work to my family. Thank you for allowing me the freedom to pursue my interests and dreams. Thank you for providing me with a life of love, support, and opportunity

ACKNOWLEDGMENTS

Thank you Dr. Ajit Bharti and Dr. Koji Ando for allowing me to participate in your research and for taking time to educate me about new experimental techniques. Each day in the lab I have felt supported and welcome. I am so grateful to have had the opportunity to learn from you.

THE EFFECTS OF CTDSP1 ON TOPOI DEGRADATION AND CELLULAR RESISTANCE TO TOPOI INHIBITOR CHEMOTHERAPY TREATMENT

EMMA SWAYZE

ABSTRACT

The anticancer drug Camptothecin (CPT) specifically targets topoisomerase I (topoI). While this class of drug is used to treat various solid tumors, CPT is only effective in 13-30 percent of the patient population. Although the mechanism of the CPT resistance pathway is not fully understood, we found cancer cells degrade topoisomerase I (topoI) in response to CPT. The observed relationship between higher basal DNA-PKcs mediated phosphorylation of topoI, rapid degradation of topoI, and resistance to CPT suggested that DNA-PKcs is a critical regulator of the phosphorylation status of topoI and the rate of topoI degradation in response to CPT. The data shows CTDSP1 (a dual phosphatase) acts as a negative regulator of DNA-PKcs. Because CTDSP1 functionality plays a role in maintaining higher basal phosphorylation levels of topoI, CTDSP1 impairment contributes to greater CPT resistance. This renders the CPT chemotherapy treatment ineffective. We hypothesized inducing the catalytically inactive form of CTDPS1 via both knockdown and inhibition experiments would increase cancer cell resistance to CPT as a result of an overactive topoI degradation pathway. The function of CTDSP1 was impaired in the two colon cancer cell lines, HCT15 and HCT116, by silencing with siRNA and using Rabeprazole (a pharmacological agent known to inhibit CTDSP1). Inhibition of CTDSP1 phosphatase activity resulted in greater phosphorylation of DNA-PKcs and increased the rate of topoI degradation in the cells in response to CPT.

Cellular resistance was also more notable in the sensitive HCT116 cell lines. HCT15 cells degrade topoI rapidly and are resistant to CPT. Thus, the effect of CPT is not as pronounced in this cell line. CTDSP1 knock down cells showed the greatest DNA-PKcs phosphorylation and topoI degradation when treated with CPT. In addition, the present study includes a clonogenic assay that shows a larger cell survival fraction in Rabeprazole treated HCT116 cells in comparison to controls after exposure to CPT. A higher survival fraction after CPT exposure is reflective of greater CPT resistance. This suggests that cell viability is enhanced during CPT chemotherapy treatment in CTDSP1 null colorectal cancer cells. Lastly, An EGFP read out experiment of topoI tagged to EGFP demonstrated CTDSP1 inhibition results in reduced topoI levels in colorectal cancer cells. The present study showed the potential link between lower topoI levels and greater resistance to CPT by showing that both effects are outcomes of silencing CTDSP1.

TABLE OF CONTENTS

LIST OF TABLES

LIST OF FIGURES

LIST OF ABBREVIATIONS

ABC transporter…….....ATP-binding cassette transporters

ATPase……Adenosine Triphosphatase

BRCA1……..Cells of breast and other tissue that respond to DNA damage

BT474 ……Human breast carcinoma cells that over express growth factor receptors

BSA…….... Bovine Serum Albumin

BU ..... Boston University

CAS9…… CRISP Associated protein 9

CALGB…… Cancer and leukemia group B

ccRCC……...Clear cell renal cell carcinoma

cDNA…… complementary DNA

cm……. centimeter

c-Myc……..V-Myc Avian myelocytomatosis Viral Oncogene Homolog

CTD…… RNA polymerase C-terminal domain phosphatases

CTDSP1……CTD small phosphatase 1

CPT……Camptothecin

CRC……Colorectal Cancer

CRISPR…… Clustered Regularly Interspaced Short Palindromic Repeats expression

DAPI…….4',6-diamidino-2-phenylindole

DNA-PKcs……DNA-Dependent Protein Kinase complex of Ku70 and Ku80

DLDSNR6……Camptothecin resistant cell line with Top1 Gly365Ser missense mutation

DLD-1……Dukes' type C, colorectal adenocarcinoma

DN…… Dominant Negative

DNA……Deoxyribonucleic acid

ECL……Enhanced chemiluminescence

EDTA……..Ethylenediaminetetraacetic acid

EGFP…….Enhanced green fluorescent protein

EGFP-P2A-Pac ……P2A-EGFP donor Addgene plasmid # 65562 from Jiu-lin Du

ELISA…….enzyme-linked immunosorbent assay

ERK…… Extracellular signal-regulated kinases

ERK1/2…… Extracellular signal-regulated protein kinases 1 and 2

G365S……Glycine substitution for serine at position 365

GERD…… Gastroesophageal Reflux Disease

GST ……Glutathione

HCT15……..Colorectal adenocarnima cells tumorigenic in nude mice resistant to CPT

HCT116……Colorectal adenocarnima cells tumorigenic in nude mice sensitive to CPT

hTOP1……..human topoI

IgG……Immunoglobulin G antibody

IHC……Immunohistochemistry

L…….Liter

MG132……...Potent proteasome inhibitor

μM……...Micromolar

μL……...Microliter

mL……Milliliter

mm……millimeter

mRNA……Messenger Ribonucleic Acid

NCCN……National Comprehensive Cancer Network

NCI……National Cancer Institute

NIH……National Institute of Health

nM……Nanomolar

nm…… Nanometer

NP40…….commercially available detergent nonyl phenoxypolyethoxylethanol

OD…….Optical Density

PBS……Phosphate-buffered saline

PBST……Phosphate-buffered saline with Tween

PCR……Polymerase Chain Reaction

pDNA-PKcs……phosphorylated DNA-dependent protein kinase

PE……..Plating Efficiency

phospho-S10…… phosphorylated at Serine 10

PML……Progressive multifocal leukoencephalopathy

PMSF…….Phenylmethane sulfonyl fluoride

Pro3…….Proline 3

PTEN……Phosphatase and tensin homolog protein

p-TopoI……...phosphorylated topoI

REST……Repressor element silencing transcription factor

RPM……Revolutions per minute

RPMI……Roswell Park Memorial Institute medium

Ser62……c-Myc is phosphorylated at Serine 62

S2056-DNA-PKcs……DNA-PKcs phosphorylated at serine 2056

S518……..Serine 518

SCLC…….....small cell lung cancer

SCP……small C-terminal domain phosphatase

SCP1……...small C-terminal domain phosphatase 1

SF……...Survival Fraction

sgRNA……Short guide Ribonucleic Acid

siRNA……...Small or short interfering Ribonucleic Acid

SN-38……...Active metabolite 7-ethyl-10-hydroxyCamptothecin

SpCas9……Saccharomyces pyogenes CRISPR associated protein 9

SWOG……...Southwest Oncology Group

TBST……trist-buffered saline and Polysorbate 20 or Tween 20

TEMED……Tetramethylethylenediamine

topoI……TopoI

topoI-EGFP……TopoI tagged to enhanced green fluorescent protein

topoI-pS10…….TopoI phosphorylated at Serine 10

Tris……Hydroxymethylaminomethane

V79……..Chinese Hamster lung cell line with high plating efficiency and short G1 phase

ZR-75-1……..Cell line from mammary gland tissue

INTRODUCTION

TopoI

Human DNA topoisomerase I (topoI) is located on chromosome 20q 11.2-13.1 and its primary function is to relieve DNA supercoiling during DNA replication and transcription (Fujimori et al. 1996). To manage the torsion caused by an advancing replication fork, topo I temporarily forms a covalent bond at the 3' terminus of DNA and produces a single strand break (Fujimori et al. 1996). The 5' end of DNA rotates freely and chaperones strand relaxation until topoI catalyzes religation of the strand. The topoI dissociates from the DNA at the end of the process (Fujimori et al.1996). TopoI plays a critical role in replication and transcription, but more importantly, has been identified as a specific target for a class of neoplastic drugs, Camptothecin (CPT) and its analogues. This class of drug is used to treat various solid tumors including colorectal cancer (CRC), small cell lung cancer (SCLC), pancreatic, and ovarian cancer.

Colorectal Cancer Chemotherapy

The most common therapies listed in the National Comprehensive Cancer Network (NCCN) guideline include Oxialiplatin based and Irenotecan based treatments for CRC (Ando et al. 2017). According to the CALGB/SWOG 80405 trial, the Oxialiplatin treatments are preferable in the United States. However, Irenotecan, a Camptothecin analogue, based treatments have the potential to be extremely successful in a subset of patients. For example, a case study in Japan evaluated a 49-year-old male demonstrating an 11.8cm, or 52%, tumor reduction after an Irenotecan based therapy (Ando et al. 2017). In order to ensure patients are receiving the best care possible, it is

necessary to determine a biomarker to establish whether patients will or will not respond to Irenotecan. Production of a biomarker will allow certain patients the opportunity to try this alternative treatment that may be vastly more successful than the Oxialiplatin treatment. Additionally, establishing a biomarker will allow physicians to avoid administering this alternative treatment to patients with resistant cells. In order to discover factors indicative of cellular resistance, it is essential to explore the mechanism of Camptothecin.

Camptothecin Mechanisms

The mechanisms of topoI inhibition by CPTs are well understood. CPTs block the DNA-re-ligation step of the topoI mediated DNA cutting and re-ligation cycle (Goldwasser et al. 1995). CPT induces cytotoxicity through binding and stabilizing DNA and topoI to form a cleavable complex (Hsiang et al. 1988). The resulting collisions with the replication fork leads to a DNA-double strand break and cell death (Liu et al. 2000). The effectiveness of CPT was tested on a variety of cell lineages and showed varying effectiveness. While some patients responded well to CPT treatment, others demonstrated resistance to the CPT drug. The response rate to CPT was only 30% in a trial conducted on patients with CRC (Arakawa et al. 2006). The ineffectiveness of CPT on certain cell lines led to an investigation of potential mechanisms of drug resistance.

Potential Mechanisms for Resistance

Many studies evaluated the possibility of a mutation of the topoI gene as the mechanism for CPT drug resistance. In an *in vitro* study, a CPT resistant sub-line of colon cancer cells DLDSNR6 was compared to CPT non-resistant DLD-1 colon cancer

cells (Arakawa et al.2006). It was determined that the resistant cells possessed a topoI gene mutation where glycine was substituted for serine at amino acid residue 365 (G365S) (Arakawa et al. 2006). While the mutation had no effect on the amount of topoI present in the cell, there was a notable decrease in catalytic ability of the mutated topoI. When treated with CPT, mutated cells produced less topoI and DNA cleavable complexes compared to non-mutated DLD-1 cells (Arakawa et al.2006). This experiment suggests that the mutation prevented topoI from producing a stable complex with DNA, which contributes to CPT resistance. Additionally, *in vitro* studies were conducted with CPT derivatives in SN-38 resistant human colon cancer cells. Results indicated that a G365S mutation hindered the ability of CPT analogues to interact with topoI at the 3' catalytic tyrosine (Arakawa et al. 2006). Although in vitro studies showed promising results for the connection between genetic mutations and CPT resistance, clinical trials showed no significant results for the relationship. Another experiment that investigated the clinical relevance of topoI mutations to CPT resistance was conducted on 127 samples from 56 patients with lung tumors (Ohashi et al.1996). In vitro point mutations that were thought to be a mechanism of CPT resistance showed no significant difference in CPT resistance in vivo. While topoI gene mutations may alter CPT binding and cause some resistance, it is not considered to be the main mechanism. Finally, data from an antidrug screen for 60 human tumor cell lines conducted by National Cancer Institute revealed no correlation between gene expression profiles and CPT drug (Scherf et al.2000).

Another avenue explored for the mechanism of CPT resistance was removal of CPT via ABC transporter. Researchers used Rhodamine as a predictive measure of anti-cancer drug response to ABC transporter expression (Lee et al.1994). Results showed ABC-B1 removes chemotherapeutic agents from cells, causing resistance to the drugs. The NCI used a PCR of cDNA to evaluate the mRNA expression of 48 human ABC transporters in 60 cancer cell lines. These cell lines were then screened for a correlation between ABC transporter gene expression and CPT response, and the results are shown in Figure 1 (Szakacs et al.2004). ABC-B1 transporters could potentially promote drug resistance if the transporters removed CPT from the cell. If CPT resistance were related to ABC transporter protein expression, low level of CPT inside the cell would be expected in the presence of transporter. The results in Figure 1 reveal CPT is not a substrate for ABC transporters including ABCB1 (Szakacs et al.2004). This suggests there is no relationship between CPT resistance and ABC-B1 expression, and thus no relationship between CPT and ABC transporters.

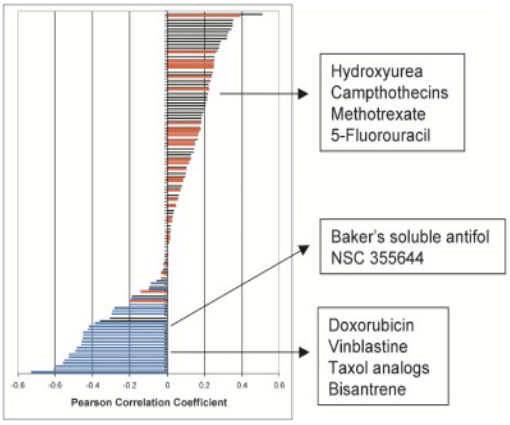

Figure 1: Adapted from the Szakacs study, Figure 1 shows the effect of ABC-B1 transporter expression on drug sensitivity in 60 cancer cell lines. Blue bars indicate low expression of drug in the presence of the ABC-B1 transporter. These drugs are substrates of the ABC-B1 transporter. In contrast, agents characterized by red bars, like CPT, are not substrates of the ABC-B1 transporter and are highly expressed inside the cell in the presence of the ABC-B1 transporter. High expression of CPT inside the cell in the presence of the transporter suggests CPT resistance is largely due to another mechanism.

A more recent alternative mechanism of resistance that has been suggested involves the rate of degradation of topoI through the ubiquitin 26S proteasome pathway

(Desai et al.2001). Studies were conducted on CPT sensitive ZR-75-1 and CPT resistant BT474 breast cancer cell lines (Desai et al. 2001). ZR-75-1 cells defective in topoI down regulation were the most sensitive to CPT and experienced apoptosis, whereas BT474 cells with the ability to effectively down regulate topoI were most resistance to CPT (Desai et al. 2001). These results suggest a relationship between CPT-induced down regulation of topoI and CPT resistance.

To further examine the mechanism of topoI down regulation on CPT resistance, a 26S proteasome inhibitor MG132 was used to inhibit topoI degradation in BT474 and V79 cell lines (Desai et al.2001). In the presence of MG132, both cell lineages experienced increased cytotoxicity from CPT and greater efficacy of the anti-cancer drug. In addition, the Bharti lab treated both sensitive HCT116 and resistant HCT15 cell lines containing topoI tagged to EGFP with SN-38, a form of CPT (Ando et al. 2017). The intensity of EGFP fluorescence was recorded at different time intervals in order to measure the degradation of topoI (Ando et al. 2017). Immunofluorescent staining shown in Figure 2 reveals the intensity of EGFP decreases after SN-38 treatment.

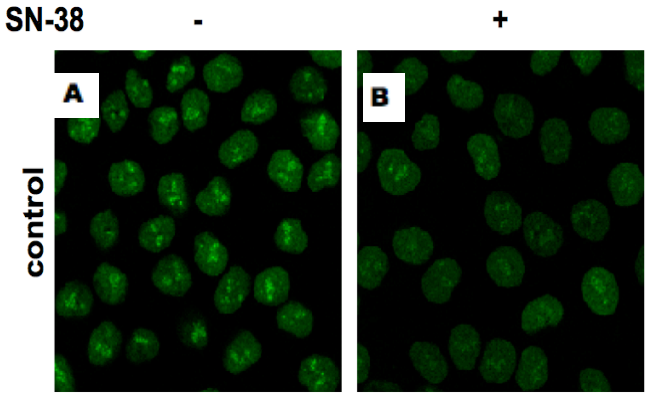

Figure 2: Adapted from the Ando study, Figure 2 reveals live imaging of topoI-EGFP in resistant cell line HCT15 with and without treatment of SN-38 (Ando et al. 2017). Greater intensity located near the nucleolus region of the cell represents topoI tagged to EGFP within the cell. Panel A, containing HCT15 cells without SN-38 exposure, shows greater intensity than HCT15 cells treated with 2.5μM SN-38 in Panel B. Greater degradation of topoI is observed in HCT15 cells after treatment with SN-38.

These results indicate treatment with SN-38 triggers the topoI degradation pathway. The more CPT resistant HCT15 cell line degrades topoI faster than the sensitive HCT116 cell line, suggesting the role of topoI degradation as a contributor to CPT resistance. Evaluating the intensity of EGFP immunofluorescence is a method of measuring the quantity of the EGFP tagged topoI in a cell that I will use in my experiments.

The link between topoI degradation and cellular resistance to CPT chemotherapy treatment has inspired researchers to examine the topoI degradation pathway shown in detail in Figure 3 (Ando et al. 2017). The rate of topoI degradation in the cell influences the cellular response to CPT. When topoI is degraded faster, CPT is less effective at destroying cells. An immunohistochemistry (IHC) experiment conducted in the Bharti lab revealed that a larger quantity of topoI is phosphorylated at serine 10 in CPT resistant colorectal cancer cells than in sensitive cell lines (Ando et al. 2017). This suggests that phosphorylation of topoI is a critical step in degradation.

Higher basal levels of serine 10 topoI phosphorylation were observed in cells demonstrating greater resistance to CPT. This relationship led the Bharti lab to investigate upstream events contributing to these resistance conditions. The Bharti lab silenced a myriad of phosphatases in order to isolate proteins influencing DNA-PKcs. After further examination of the topoI degradation pathway, CTDSP1 and PTEN were identified as upstream candidates influencing the phosphorylation and activation of DNA-PKcs. When silenced CTDSP1 and PTEN were unable to remove the phosphate from DNA-PKcs (Ando et al. 2017). Phosphorylation of DNA-PKcs activates the kinase

to phosphorylate other proteins including topoI. Post phosphorylation, topoI is ubiquitinated and subsequently degraded.

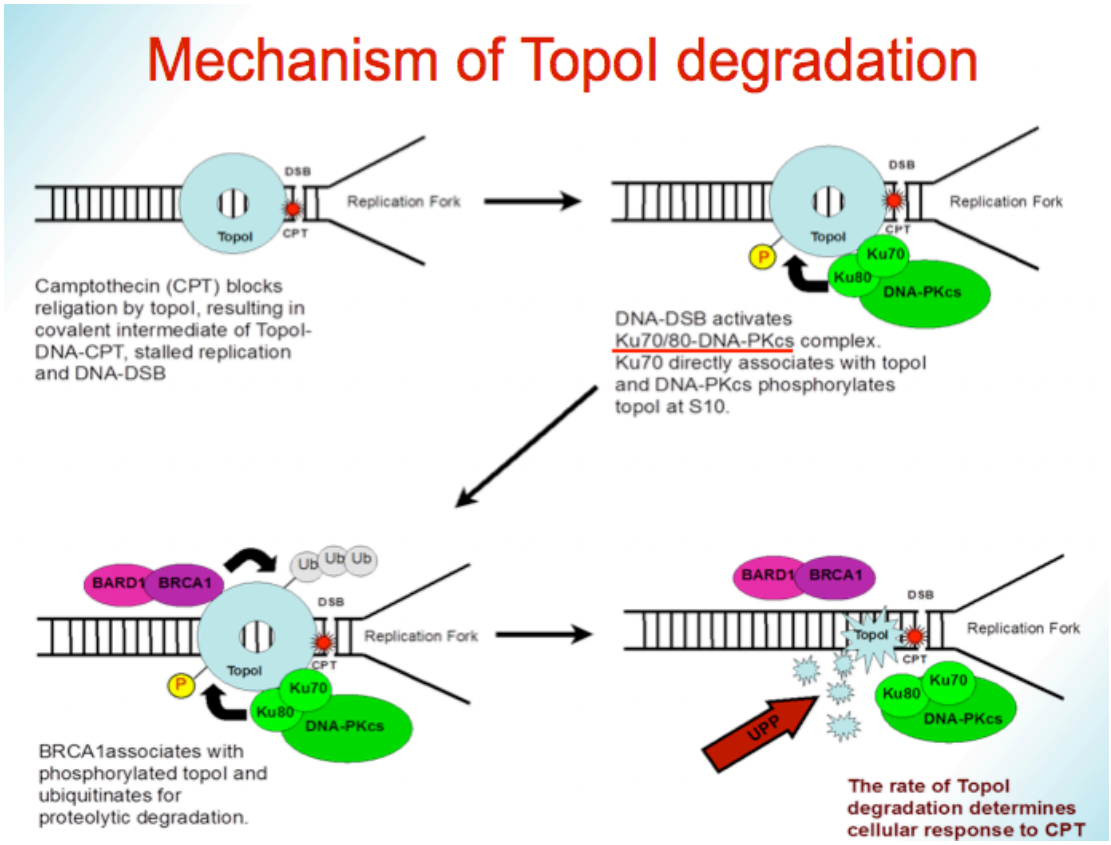

Figure 3: Adapted from the Bharti lab, Figure 3 shows the degradation pathway of topoI (Ando et al. 2017). When phosphorylated, DNA-PKcs is activated to phosphorylate topoI. BRAC1 interacts with and ubiquitinates phosphorylated topoI, initiating the proteolytic degradation pathway. When topoI is degraded by the proteasome, CPT has no substrate to interact with and is no longer an effective therapeutic agent.

Silencing of phosphatases PTEN and CTDSP1 shows both proteins also play a role in topoI degradation. The Bharti lab administered an siRNA library screening to nuclear phosphatases where 56 nuclear phosphatase genes were silenced by siRNA and then treated with SN-38 (Ando et al. 2017). EGFP tagged topoisomerase was then measured at various time intervals. Figure 4 demonstrates the differences in

immunofluorescent staining with anti-topoI-antibody between cells under control conditions and after knockdown of PTEN. Cells with PTEN knocked down demonstrated less immunofluorescence, indicating greater topoI degradation in the CPT treated cells (Ando et al. 2017).

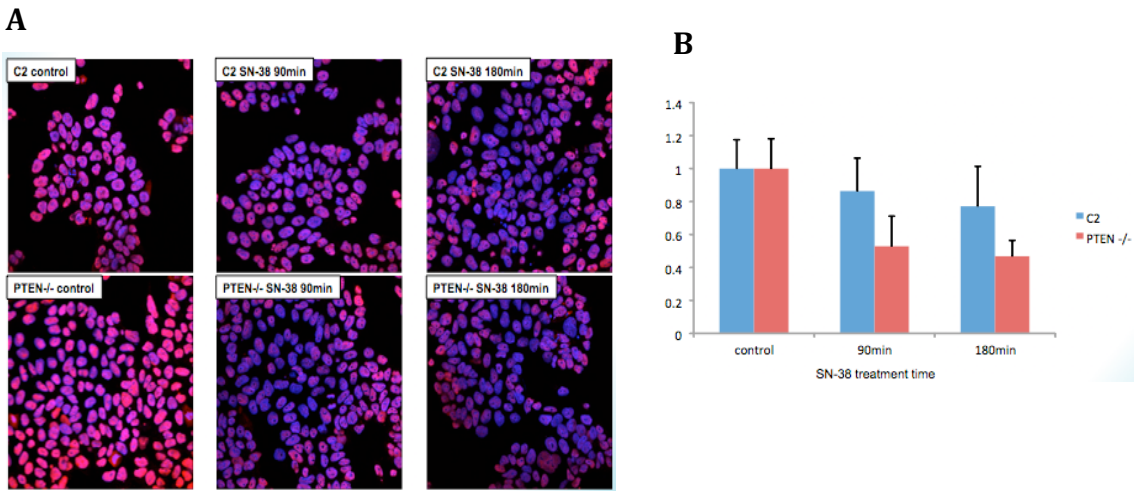

Figure 4: Adapted from the Bharti lab, Figure 4A shows immunofluorescent staining of cells with PTEN compared to PTEN knock out cells after exposure to SN-38 for different time intervals (Ando et al. 2017). Greater immunofluorescence reflects a greater amount of topoI in the cell. Less intensity is notable in PTEN knockout cells treated with SN-38 for both 90 and 180 minutes. Figure 4B shows the measurement of topoI immunofluorescence intensity using ImageJ software. Because intensity levels reached the lowest point in PTEN knockout cells exposed to SN-38 for 180 minutes, topoI degradation was the greatest in these cells relative to the control.

Knocking out PTEN not only enhances breakdown of topoI, but also increases cellular resistance to CPT. After plated cells with both functional and knocked down PTEN were treated with SN-38 for 24 hours, the cells without PTEN exhibited greater proliferation (Ando et al. 2017). The Bharti lab further explored the mechanism of PTEN in the topoI degradation pathway in order to understand how the protein confers cellular resistance to SN-38. A DNA-PKcs kinase assay revealed that DNA-PKcs is

dephosphorylated by PTEN (Ando et al. 2017). When PTEN is non-functional, there is greater phosphorylation of DNA-PKcs, which leads to greater topoI phosphorylation and then degradation. Figure 5 shows the influence of PTEN on the topoI degradation pathway (Ando et al. 2017). Because PTEN knockdown cells are more resistant to SN-38, greater phosphorylation of DNA-PKcs may be another indicator of cellular resistance to CPT. Factors such as greater DNA-PKcs phosphorylation, lower levels of topoI, and non-functional PTEN serve as predictive biomarkers for cellular resistance to CPT colorectal cancer chemotherapy treatment. Phosphorylation of topoI by pDNA-PKcs marks topoI for ubiquitination followed by degradation, making cells resistant to CPT. In my experiment, I will be looking at the phosphatase CTDSP1 identified in the siRNA screening to determine whether CTDSP1 influences cellular resistance to CPT in a similar manner to PTEN. The Bharti lab generated an antibody against topoI phospho-S10 that will be used in my IHC experiment to examine the levels of topoI after knocking out CTDSP1 (Ando et al. 2017).

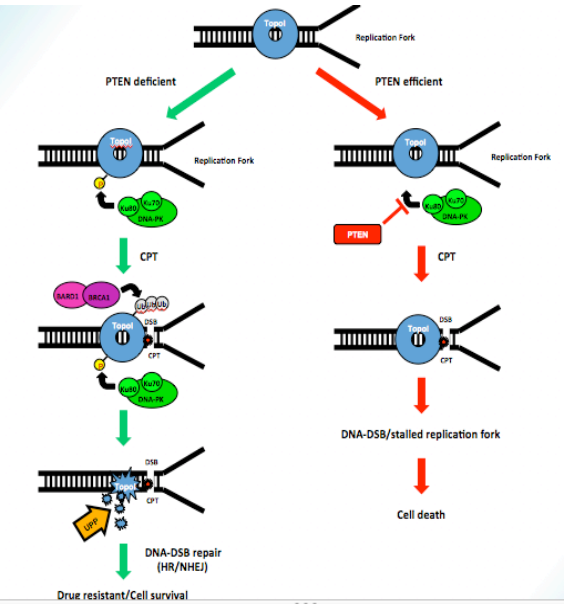

Figure 5: Adapted from the Bharti lab, Figure 5 shows the role of PTEN in the topoI degradation pathway (Ando et al. 2017). When PTEN is not present in the cell, DNA-PKcs remains phosphorylated and is able to phosphorylate topoI. Phosphorylation of topoI recruits BRCA1 and associated proteins that ubquitinate and initiate topoI degradation. CTDSP1 is hypothesized to perform a similar function to that of PTEN and may also influence the topoI degradation pathway leading to cellular resistance to CPT.

CTDSP1 and CPT Resistance

CTDSP1 plays a similar role to the phosphatase PTEN. The phosphatase PTEN is known to remove the phosphate from DNA-PKcs, which is then activated to phosphorylate topoI, leading to the subsequent degradation of topoI. CTDSP1 is a serine/threonine phosphatase that is part of the SCP protein family (Lin et al. 2014). Proteins belonging to the SCP family dephosphorylate at the C terminal domain of proteins (Lin et al. 2014). Additionally, loss of function of these phosphatases has demonstrated an increase in tumor formation and proliferation for several types of cancers including clear cell renal cell carcinoma (Kashuba et al. 2004). The Lin study demonstrated overexpression of CTDSP1 in ccRCC cell lines 786-O and A-498 (Lin et al. 2014).

CTDSP1 has also been shown to regulate the stability of the transcription factor c-Myc. Enhanced expression of c-Myc is correlated with tumorigenesis (Wang et al. 2015). Similar to topoI, c-Myc stability is also regulated by phosphorylation. CTDSP1 inhibits c-Myc mediated phosphorylation via dephosphorylating a serine 62 residue (Wang et al. 2015). Figure 6 demonstrates that wild-type CTDSP1 reduces c-Myc phosphorylation at Ser62, whereas a catalytically inactive mutant of CTDSP1 does not influence c-Myc phosphorylation (Wang et al. 2015). This suggests that CTDSP1 is responsible for direct dephosphorylation at the Ser62 residue on c-Myc.

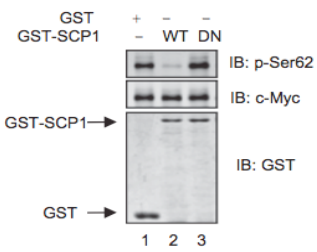

Figure 6: Adapted from the W. Wang study, figure 6 shows that in the presence of catalytically active wild type GST-SCP1 (also referred to as CTDSP1) the serine 62 residue of c-Myc does not undergo phosphorylation. The DN non-catalytically active

version of GST-SCP1 does result in phosphorylation of c-Myc. This suggests that the presence alone of GST-SCP1 is not enough to remove the phosphate from c-Myc. Catalytic activation of GST-SCP1 is essential for dephosphorylation effects to occur.

The Wang study examines the levels of c-Myc in the presence of both CTDSP1-WT and the inactive CTDSP1 mutant using a western blot. Results indicate CTDSP1 is a negative regulator of c-Myc, for in the presence of the wild type CTDSP1, levels of c-Myc protein are reduced. In my experiment, I use the western blotting technique to assess the amount of various proteins after both inhibiting CTDSP1 with Rabeprazole and knocking down CTDSP1 with siRNA. To explore the physical interaction between CTDSP1 and the substrate c-Myc, a pull down assay using glutathione S- transferase was conducted. Results revealed that both wild type and catalytically inactive mutant CTDSP1 directly interacted with c-Myc (Wang et al. 2015). Therefore, the direct interaction between the two proteins occurs regardless of the phosphatase activity (Wang et al. 2015).

The previous experiments suggest the role of CTDSP1 as a phosphatase that regulates proteins involved in the topoisomerase degradation pathway at a serine residue located near the C-terminal domain. Before knocking down CTDSP1 using siRNA, experiments were conducted using an inhibitor of CTDSP1. Inhibitors of phosphatases from the Scp family like CTDSP1 were screened in a pilot library of the NIH clinical collection and spectrum collection to assess for ability to inhibit CTDSP1 specifically. Results indicated Rabeprazole would serve as an inhibitor for CTDSP1 (Zhang et al. 2011). To better understand the interaction between Rabeprazole and CTDSP1, X ray data collection was conducted in the Zhang study on Scp1 crystals (PEG-based

conditions) soaked in 0.5mM Rabeprazole for 2-3 hours (Zhang et al. 2011). Figure 7 reveals maximum interaction between the hydrophobic recognition pocket of CTDSP1 and the Pro3 residue of Rabeprazole (Zhang et al. 2011).

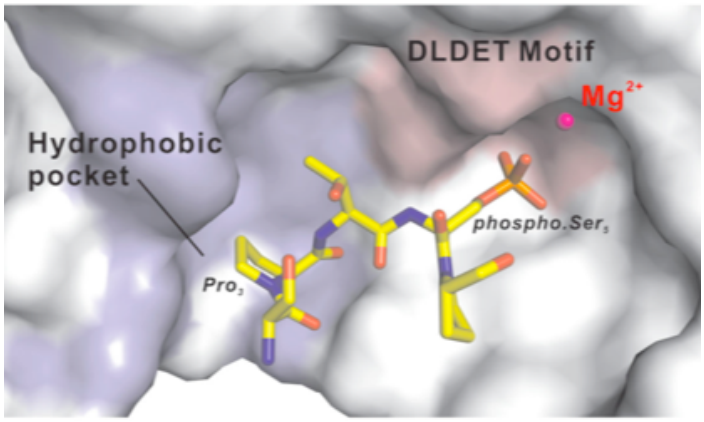

Figure 7: Adapted from the Zhang study, Figure 7 shows a 3D model of the interaction between the Pro3 residue of Rabeprazole and the hydrophobic binding pocket of Scp1.

A mutagenesis experiment around the hydrophobic binding pocket examined the ability of Rabeprazole to inhibit CTDSP1 when the hydrophobic binding pocket was altered (Zhang et al. 2011). Results suggest that when the hydrophobic binding pocket of CTDSP1 is mutated, the ability of Rabeprazole to inhibit the phosphatase is decreased, suggesting the hydrophobic binding pocket is critical for the interaction of the two molecules.

In current medical practice, Rabeprazole has been used to treat peptic ulcers and GERD by targeting and irreversibly inhibiting proton exchange via the hydrogen potassium ATPase (Gu et al. 2014). While the mechanism for proton pump inhibition is through a covalent bond, Rabeprazole non-covalently binds Pro3 of the CTD peptide in the hydrophobic binding pocket of CTDSP1 (Zhang et al. 2011). Additionally, when treated with Rabeprazole, gastric cancer cells experienced reduced viability. Typically,

gastric cancer cells have an extremely active proton pump and ability to eradicate protons within the cell. Rabeprazole inhibits the pump in gastric cancer cells, which creates an extremely acidic environment within the cancer cell that leads to cell death (Gu et al. 2014). The Gu study also shows Rabeprazole inhibits the phosphorylation of ERK1/2 (Gu et al. 2014). Without phosphorylation of ERK1/2, the signal transduction pathway that ERK1/2 initiates was suppressed, leading to induction of apoptosis in gastric cancer cells (Gu et al. 2014). ERK phosphorylation leads to degradation of repressor element silencing transcription factor (REST), a compound that stunts neurogenesis (Nesti et al. 2014). Therefore CTDSP1 is responsible for stabilizing REST and preventing growth and differentiation from occurring. In addition, preventing phosphorylation at S861/864 residues located near the C terminus of the REST led to increased stability of REST (Nesti et al. 2014). ERK1 and 2 are kinases responsible for phosphorylation of REST at S861/864 residues that enhance growth. Based on the results of these experiments, it is possible CTDSP1 may influence DNA-PKcs in a similar manner to REST. Normal CTDSP1 may prevent proline-directed phosphorylation at C terminal serine residues of DNA-PKcs. In my experiments, I will both knock down CTDSP1 with siRNA and inhibit CTDSP1 with Rabeprazole. Previous research suggests the amount of phosphorylated DNA-PKcs will increase and the amount of topoI will decrease when CTDSP1 is non functional

SPECIFIC AIMS

In order to determine whether downregulation of CTDSP1 contributes to cellular resistance to CPT chemotherapy agents, the specific aims of this study were:

1. To observe the role of CTDSP1 in the topoI degradation pathway after both inhibiting CTDSP1with Rabeprazole and then knocking down CTDSP1with siRNA.
2. To determine the cellular response to CPT after CTDSP1 inhibition.
3. To determine the change in the rate of CPT induced topoI degradation in CPT sensitive cell lines.

METHODS

Developing topoI-pS10 phosphospecific monoclonal antibody: The hybridoma core facility of the Dana-Farber Cancer Institute located in Boston provided a mouse monoclonal antibody that detected topoI-pS10. The antibody was created using a phosphopeptide with the N terminus of topoI with phosphoserine 10. After ELISA assays were conducted, 10 clones were selected to use for immunohistochemistry experiments. Clone 3573.1C1.H5.H7 was selected for large volume culture and antibody purification (Ando et al. 2017).

Generating the topoI-EGFP HCT15 cell lines: Plasmids were used to create different HCT15 cell lines. Single guide-RNA (sgRNA) targeted the topoI stop codon. The goal of the sgRNA was to destroy the *Streptococcus pyogenes* Cas9 (SpCas9)-VQR variant binding site after the gene was changed (Kleinstiver 481-5). An EGFP-P2A-Pac fusion cassette was used to make the homology regions from HCT15 cells 5' and 3' of the topoI stop codon. The purpose of using this cassette was to ensure puromycin resistance and to create the donor plasmid used in the experiment. Lipofectamine (Lifetechnology) was used to transfect the HCT15 cells. PCR amplifying of the genomic locus and sequencing, western blot analysis, and immunofluorescence were used to confirm that the genome-editing cassette was successfully inserted in the single cell cloned HCT15 *hTOP1*-EGFP cells. Descriptions of other procedures such as DNA-PKcs kinase assays are provided in supplementary procedures in the Ando paper (Ando et al. 2017).

Editing EGFP in downstream of TopoI: CRISPR/CAS9 genome editing technology was used to place the EGFP gene after the hTOP1 gene coding for topoI. The procedure is demonstrated in figure 8 below.

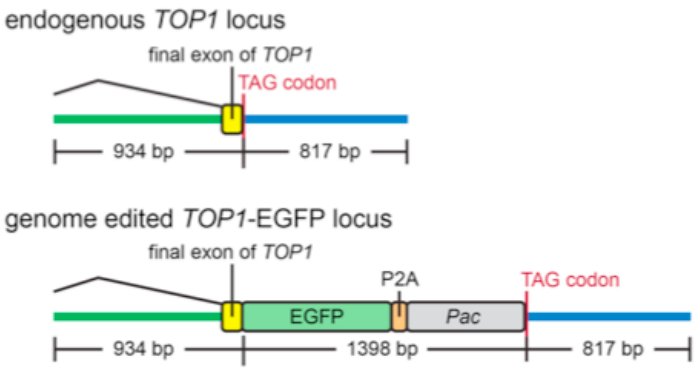

Figure 8: Genomic editing procedure for tagging TopoI to EGFP via insertion into mRNA adapted from *Nature* 2015, *Science* 2014

CTDSP1 Inhibitor Experiments

After culturing both resistant cell line HCT15 4E7 and sensitive cell line HCT116 12-G10 in two different flasks, the cells were first split.

Cell Splitting: First, the RPMI 1 µg/mL puromycin media and RPMI 2µg/mL puromycin media were aspirated from flasks containing HCT116 12-G10 and HCT15 4E7 cells respectively. Aspirations were done two times, and then the media was discarded in a waste bucket.

After the addition of 2mL of trypsin, each flask was placed in an incubator for 5 minutes. Two new tubes were prepared and labeled for each cell line. The trypsin treated flasks were removed from the incubator and 6mL of RPMI media was added to each flask. The cells were then collected from each flask and put into the new tubes. The new

tubes were then centrifuged for 1,500 rpm 5 minutes. Once the tubes were centrifuged, cell pellets were visible and the media in each tube was dumped into the waste bucket. 5mL of fresh RPMI was added into the tubes with cell pellets. The tubes were then vortexed.

Three 6cm dishes with 0μM, 5μM, and 10μM concentrations of Rabeprazole were prepared for both cell lines HCT16 4E7 and HCT115 1-2G10. Rabeprazole was ordered from Sigma under the catalogue number 1478505. Untreated RPMI media was added to the 0μM Rabeprazole plates. To create a 5μM concentration of Rabeprazole in RPMI, 50μL of 1mM Rabeprazole was added to 10mL of RPMI. To create a 10μM concentration of Rabeprazole in RPMI, 100 μL of 1mM Rabeprazole was added to 10mL of RPMI. 3mL of each solution were added to their respective 10cm Dishes. A 1:10 ratio for cells to mL of RPMI was used to assess how many cells to put into the flask. For every 1mL of RPMI, 100μL cells were added. Since 5mL of RPMI solutions were added to each tube with the cell pellet, 500μL of cells from the tube with the vortexed cell pellet were added to each 6cm dish. All dishes were placed in the incubator overnight.

In addition to the 6cm dishes shown in table 1, two new flasks were prepared for each cell line. For cell line HCT15 4E7, 10mL of RPMI with 2μg/mL amount of puromycin was added to the flask. For cell line HCT116 12-G10, 10mL of RPMI with 1μg/mL amount of puromycin was added to the flask. 500μL of cells from the tubes with cells vortexed in 5mL of RPMI were added to their respective flasks. Both flasks were placed in the incubator for a week to sustain the cell lines before being split again.

Treating cells with SN-38*:* The newly prepared 6cm dishes were removed from the incubator after a 72-hour period. A 2.5μM concentration of SN-38 was added to the 3 dishes with cell line HCT15 4E7. To prepare this concentration of SN-38, 25μL SN-38 was added 10mL of RPMI**.** 3mL of the SN-38 and RPMI solution were added to each HCT115 dish, and the dishes were placed in the incubator for 30 minutes. A 250nM concentration of SN-38 was added to the 3 dishes with cell line HCT116 12-G10. To prepare this concentration of SN-38, 2.5μL SN-38 was added 10mL of RPMI**.** 3mL of the SN-38 and RPMI solution were added to each of the HCT116 12-G10 dishes. Dishes were placed in the incubator for 60 minutes.

Cell Lysate Buffer Preparation*:* The cell lysate buffer used in the experiment contained150mM NaCl, 50mM Tris (pH 7.5), 1% NP40, 1mM DTT, 1mM EDTA, 50 μL NaF, 50 μL NaV, 50 μL PMSF, 50 μL Pepstatin, and 50 μL Aprotinin as shown in table 2 of the appendix..

The amount of cell lysate buffer was adjusted to achieve the same concentrations listed in table 3 of the appendix in a 10mL volume.

Preparing Cell Lysates: First, all dishes were removed from the incubator and placed on ice. The media from each dish was then aspirated and discarded in the waste bucket. 1mL of PBS was placed into each dish to wash the cells. The PBS was then aspirated and discarded using the 1000μL pipette. 150μL of lysate buffer was added to each dish. After adding the lysate buffer, a cell scraper was used to scrape the cells off the plates and collect the cells and buffer mixture into 6 newly labeled microtubes using the 1000μL pipette. All microtubes were incubated on ice for 30 minutes once filled with the cell

lysate mixtures. The 6 microtubes were vortexed and then centrifuged for 15 minutes in 14,000 RPM, at 4°C. The supernatant was then collected from the microtubes and put into newly labeled microtubes using the 200µL pipette in order to avoid collecting the pellet.

Examining the Concentration of the Cells in the Lysate: We prepared the following seven microtubes show in table 4 of the appendix. 800µL of water and 200µL Biorad Protein assay were added to each tube. 2.5µL of the previously prepared lysis buffer was added to the control tube. 2.5µL of each sample was put into their respective microtubes. Each tube was then vortexed. A change in color from brown to blue indicates protein from the sample is in the microtube. Contents from the microtube were transferred to cuvettes and placed in a spectrophotometer. The spectrophotometer measures the absorption of light in the samples compared to the lysate buffer in order to determine the concentration of protein in each sample. The absorbance of light of each sample was measured at 560nm. The cuvette with lysate buffer was first placed into the spectrophotometer to use as a blank. Then the remaining samples were placed into the spectrophotometer and the protein concentrations were recorded as OD values.

***Western Blot Analysis*:** When examining DNA-PKCS, a 5 % gel was prepared. When examining topoI, a 7.5% gel was prepared. The Materials used to create a 5% and 7.5% gel can be found respectively in table 5 and 6 of the appendix. When examining topoI, a 7.5% gel was prepared.

While waiting for 45 minutes for the gel to solidify, 1L of running buffer solution was prepared using 100mL of 10X running buffer and 900mL of water. 1L of transfer

buffer solution was prepared as well. In a 1000mL-graduated cylinder, we added 100mL of 10% methanol, 100mL of 10X transfer buffer, and 800mL of water. After covering the graduated cylinder with a parafilm, the solution was put into a cold room at 4° Celcius for an hour. After the separating gel hardened, the indicated amount of TEMED was added to the stacking gel and the comb inserted into the gel. After 20 minutes, the wells were ready to load.

***Preparing the Samples*:** Lysate samples stored in the -80° freezer were thawed on ice for one hour. After thawing was complete, the samples were vortexed. The concentrations of each sample were determined using the spectrophotometer, and calculations were done to determine the amount of each sample to load into the Western blot.

***Calculations to determine the quantity of each lysate to use in Western Blot**:* The OD values of each sample were compared and the following equation was used to determine the µL amount of each sample to add to the western blot.

Equation 1: [Lowest OD value of all samples/OD value of sample] * 10= (__) µL

Making the Western Blot Lysate Buffer: 10% DTT and 90% Lameli sample buffer were used to prepare a 100µL solution. 90µL of Lameli sample buffer and 10µL of 1M DTT stored in the -20°C freezer were added to a microtube. The newly prepared lysate buffer and samples were added to each tube in a 1:1 ratio. The amount of sample added to each microtube was determined by the previous equation using OD values. After adding both samples and lysate buffer to microtubes, the microtubes were boiled for 5 minutes and then put on ice.

Loading the Samples and Electrophoresis: The electrophoresis apparatus was assembled, and running buffer was poured in between the two glasses containing the gel. 5μL of molecular weight marker were added to the first and last wells on the gel. The remaining samples mixed with lysate master mix were added to the wells in between. Table 7 of the appendix shows the quantity of sample and marker added to each well of the western blot gel.

The remaining running buffer was poured into the apparatus to reach a level that completely covered the samples but did not surpass the buffer between the two glass plates. The apparatus was plugged into a BioRad 200 power source at 50mV for approximately 2 hours. At this point the blue dye had just completed running off the gel and was ready to be transferred. The purpose of the electrophoresis was to separate the proteins by molecular weight.

***Transferring the Membrane*:** After completing the protein separation based on size using gel electrophoresis, the proteins on the gel were transferred to an Immobilon-P Transfer membrane, pore size 0.45μm (Millipore, Billerica, MA) using a wet transfer system (BioRad, Hercules. CA). To activate the membrane, the membrane was placed in methanol for one minute and then placed in transfer buffer for 5 minutes. Post membrane activation, a transferring cassette sandwich was assembled in the following order starting on the black side of the cassette: sponge soaked in transfer buffer, 3 pieces of filter paper, gel, immunoglobulin membrane, 3 pieces of filter paper, sponge soaked in transfer buffer. The cassette was placed in the transfer apparatus and connected to a Biorad Powerpac 300 apparatus. For a DNA-PKcs western blot, the settings were adjusted to

200milliAmps, and the transfer occurred for 2 hours in the 4-degree cold room. For a topoI western blot, the settings were adjusted to 10milliAmps, and the transfer occurred over night in the 4° cold room.

Membrane Blocking: To block the DNA-PKcs membrane, the newly transferred membrane was soaked in 2% BSA/TBS-T for 1 hour on a rocker. To prepare 2% BSA, 1g of Albumin Bovine Serum was vortexed with 50mL of 0.05% TBS-T. To block the topoI membrane, the newly transferred membrane was soaked in 5% skim Milk and 0.05% PBS-T solution for 1 hour. To prepare this solution 2.5g of Biorad blotting grade buffer was vortexed with 50mL of 0.05% PBS-T.

***Applying the Primary Antibody*:** 10mL of a primary antibody solution containing anti-S2056-DNA-PKcs was added to the DNA-PKcs western blot. The membrane covered by primary antibody was placed on a rocker in the 4°C cold room overnight. 10mL of primary antibody solution containing anti-topoI and anti-βactin was applied to the membrane measuring topoI for one hour in a room temperature room on a rocker.

***Washing the Membrane*:** When using a DNA-PKcs membrane, the membrane was soaked 3 times for a period of five minutes in 0.05% TBS-T solution. This buffer is used when trying to detect phosphoproteins because we do not want to block phosphate when trying to measure DNA-PKcs. To prepare TBS-T, we added 500mL of transfer buffer, 50mL of 10X TBS, 450mL of distilled water, and 250µL of Tween20. A stirring bar was added to the graduated cylinder containing the solution, and the cylinder was covered with a parafilm. When using a topoI membrane, the membrane was soaked for a period

of 5 minutes in a 0.05% PBS-T solution. To prepare PBS-T, we added 500mL of transfer buffer, 50mL of PBS, 450mL of distilled water, and 250µL Tween. A stirring bar was added to the graduated cylinder containing the solution, and the cylinder was covered with a parafilm.

Applying the Secondary Antibody: 3µL of rabbit anti-human IgG secondary antibody stored at 4°C was diluted with 9mL 2% BSA/0.05% TBS-T. The dilution was added to the DNA-PKcs membrane for one hour. 3µL of mouse anti-human IgG secondary antibody stored at 4°C was diluted with 9mL 5% milk/0.05% PBS-T. The dilution was added to the topoI membrane for one hour. The same solutions previously discussed were used to wash their respective membranes after applying the secondary antibody. For the DNA-PKcs western blot, washes were conducted for two 15-minute intervals followed by one half hour interval. For the topoI western blot, washes were conducted for three 10-minute intervals.

***Developing the Membrane*:** A developing solution was prepared using 800µL of Western Lighting Plus ECL oxidizing reagent plus and 800µL of Western Lighting Plus ECL enhanced luminol reagent plus. The membrane was sprayed with the developing solution and left to sit on a piece of seran wrap for 1 minute. The membrane was then covered with a dry piece of seran wrap and then taped inside a Biorad exposure cassette. The cassette containing the membrane was taken to a dark room to be developed. For the DNA-PKcs membrane, film was placed into the box for 1 minute 30 seconds. The film was then removed from the box, flipped upside down, and placed into the box for 2

minutes. The film was then removed again and placed in the film developer. For the topoI membrane, the film was placed into the box for 1 second. The film was then removed from the box, flipped upside down, and placed into the box for 2 seconds. The film was then removed again and placed in the film developer. After 4 minutes, the developer spits out completed films with visible bands.

***Clonogenic Assay*:** All materials including plates and pipettes used were sterile. RPMI medium and trypsin were warmed at 37 °C for one hour. The media was aspirated from a flask of newly grown cells x2 and discarded in the waste bucket. 2mL of Trypsin was then put into the flask of HCT116 cells. The flask was then placed into the incubator for 5 minutes. 6mL of RPMI media was then added to a fresh tube labeled HCT116-1-2G10. The tube was then centrifuged at 1,500 RPM for 5 minutes. After centrifuging the tube, the media was dumped out into the waste bucket, leaving a cell pellet at the bottom of the otherwise empty tube. 5mL RPMI was added into the tube with cell pellet. The tube was then vortexed until the cell pellet was completely dissolved in the added media. Table 8 of the Appendix shows the contents of the 10cm plates of HCT116-1-2G10 cells cultured in different Rabeprazole and SN38 conditions.

10 mL of RPMI medium was put into plate 1 and 3. These plates contained 0μM Rabeprazole. A tube of 20mL RPMI with 200 μL of Rabeprazole was prepared. 10mL of this solution was added into Plate 2, and 10 mL of this solution was added into plate 4. These dishes contained 10μM Rabeprazole. Put 200 μL of HCT116-1-2G10 cells were added into each dish. All dishes were placed into the incubator for 4 days. After 4 days, the 4 plates of cells were divided into two sets of the following 6 well plates and exposed

to different concentrations of SN-38 shown in table 9 of the Appendix. 10mM concentration SN-38 was used in the following experiment. The contents of the 6-well plate with 10μM Rabeprazole treated 12-G10 cells are shown in table 10 of the Appendix.

150μL of 1mM Rabeprazole was put into a tube with 15mL of RPMI to create achieve a concentration of 10μM Rabeprazole. SN-38 concentrations were then put into the Rabeprazole treated RPMI. After treatment with SN-38 for 22 hours, the cells were counted.

Counting the cells: After removing the dishes of both treated and non-treated cells from the incubator, the media was aspirated and removed from each dish. Cells were then split from each of the 6 well plates into 12 cell pellets. After 5 minutes of treatment with 0.5mL of trypsin, 3mL of RPMI were added to collect and centrifuge the cells. After centrifuging the cells, the media was dumped out and 1mL of fresh RPMI was added to 12 microtubes. 800μL PBS, 100μL trypsin, and 100μL of cells were added to 12 new microtubes. Cells were then counted under the microscope. Before examining cells under the microscope on the slides, the medium with cells was pipetted up and down in order to further detach the cells. Cell counting data is shown in table 11-14 of the Appendix.

After counting the cells, six 6-well dishes were created: 3 for control 0μM Rabeprazole and 3 for 10μM Rabeprazole. The goal was to add 10 cells/1μL to the assigned dish, and in each well there was a total of 5μl of media.

The dishes were then placed in the incubator for 50 hours and then the formation of clones was assessed.

***Immunofluorescent Staining of pDNA-PKcs*:** A 6-well dish was created using the HCT116 cell line exposed to different concentrations of Rabeprazole. The contents of the 6 well-dish are shown in table 15 of the Appendix. 50µL Rabeprazole were put into in 5mL RPMI media to achieve a 10µM concentration of Rabeprazole. After filling the wells with media, a slide was placed at the bottom of each dish. After four days of treatment, the cells were prepared for immunofluorescent staining.

Fixing the Cells

After aspirating and discarding the media, the dishes were washed twice with 1mL of PBS. 1mL of 3.7% Formaldehyde was then added to each dish for a 15-minute period.

Permeabilizing the cells

The Formaldehyde solution was then aspirated and washed twice with 1mL of PBS. 1mL of 0.2% PBS-T was then added to each well for a 10-minute period. The 0.2% PBS-T was then aspirated and washed twice with 1mL of 0.01% PBS-T.

Blocking the cells

1 mL of 3%BSA/0.01% PBS-T was added to each well for one hour.

Adding the primary antibody: anti pDNA-PKcs and p-TopoI

200µL 3% BSA/0.01% PBS-T and 400µL 0.01%PBST were added to a microtube to make a 600µL 1% BSA/0.01% PBS-T solution. A western blot gel square was placed on top of the western blot wash square. Both squares combined were placed in a larger wash box and a parafilm was placed on top of the western blot wash square. 6 µL of primary antibody were placed into the 600µL microtube solution to achieve a 1:100 concentration.

Four 100µL dots of the solution were pipetted on to a parafilm. The 4 slides from the 6-well plate were placed on a 100µL dot for 1 hour.

Adding the secondary antibodies: α-Rb-Green, α-MS-Red

The slides were removed from the parafilm and placed back in their respective wells of the 6-well plate. All slides were washed twice with 0.01%PBST for 5 minutes. 200µL 3% BSA/0.01% PBS-T and 400µL 0.01%PBST were added to a microtube to make a 600µL 1%BSA/0.01% PBS-T solution. 1.2µL secondary antibody was added to the 600µL solution to achieve a 1:500 concentration. Four 100µL dots of the solution were pipetted on to a parafilm. The 4 slides from the 6-well plate were placed on a 100µL dot for 45 minutes.

Adding DAPI

The slides were placed back into the wells. 0.1% concentration of DAPI, 4',6-diamidino-2-phenylindole, was added to each well.

Mounting the cells

4 drops of Prolong Diamond Antifade mounting medium were added to a parafilm. The slides were placed on the parafilm with the cells facing the drop. After 24 hours the cells were ready to be viewed under the microscope.

***Image of topoI-EGFP*:** HCT116 cell lines with topoI-EGFP fusion proteins were incubated with 0,5, and 10µM Rabeprazole concentrations. Generation of topoI-EGFP fusion proteins was discussed earlier in the methods section. After 4 days, cells were visualized under the Leica S5 confocal microscope to examine the effects of Rabeprazole on topoI levels. Cells containing topoI tagged to EGFP revealed a bright green color.

CTDSP1 Knock Down Experiments

Dharmacon siRNA Resuspension: First, we acquired 5nmol CTDSP1(58190) siRNA capable of knocking out CTDSP1 from Dharmacon Pharmaceuticals. We then centrifuged the tube of siRNA powder. In order to prepare a 20μM stock of the siRNA suspension, we added 50μL of 5x siRNA buffer and 200μL of Nuclease free water to the tube. siRNA Resuspension volumes and concentrations are shown in table 16 of the appendix.

We pipetted the solution up and down four times and let the solution mix in the Eppendorf Mixer 5432 for 30 minutes. After centrifuging, we added 25μL of the siRNA suspension into ten individual microtubes to attain a 250nM concentration. The microtubes were then centrifuged and the siRNA concentration was confirmed using UV spectrophotometry at 260nm. 1μM of siRNA is equal to 13.3ng/μL. We achieved a reading of 249.5ng/μL for a 5nmol amount of siRNA. We then placed the CTDSP1 siRNA in the -20°C freezer overnight.

Transfecting the Cells: We plated cell lines HCT116 and 12-G10 and waited until cell growth was 70-90% confluent. Two 6-well dishes shown in table were prepared for each cell line. The contents of each dish are shown in Table 17 and Table 18 of the Appendix. 500μL of RPMI and 4μL of Lipofectamine 3000 Reagent were added to each of the four wells. 1.5μL of 20μM CTDSP1 siRNA was added to two wells of the 6-well dish for each cell line. After waiting 20 minutes, we then added 50μM cells to their respective 6-well dishes. Once the cells were added, we waited 48 hours for the cells to incubate in the

transfection materials. Once the cells were added, we waited 48 hours for the cells to incubate in the transfection materials.

Lysate Preparation: We then treated two wells from each 6-well plate with SN-38. One well treated contained siRNA, and one well treated contained no siRNA to act as a control. We prepared the following lysates for the CTDSP1 knock down experiments using the same methodology as the CTDSP1 inhibitor experiments discussed previously. Cell lines with and without functional CTDSP1 were evaluated in both control conditions and after exposure to SN-38. The lysates prepared are shown in table 19 of the Appendix. After preparing the lysates, we measured concentration of protein in the lysates using the same methods discussed previously.

***Western Blot Analysis*:** We conducted three types of western blots for CTDSP1 knock down experiments. Like the CTDSP1 inhibitor experiments, we looked at the amount of DNA-PKcs phosphorylation and topoI. We also conducted the additional western blot to confirm the knockdown of CTDSP1 in both HCT116 and 12-G10 cell lines. When examining DNA-PKcs, a 5 % gel was prepared. When examining topoI, a 7.5% gel was prepared. Lastly, when checking for the presence of CTDSP1, a 10% gel was prepared. Materials used to create the 10% gel are shown in table 20 of the Appendix. The same methods used for the inhibitor experiments were used to produce the CTDSP1 knockdown western blots. For the western blot determining whether or not CTDSP1 was successfully knocked down in each cell line, we used the primary antibody anti-CTDSP1. All other conditions for this western blot were identical to those used for topoI western blots.

Immunofluorescent Staining of pDNA-PKcs: The same methods used in the inhibitor experiments were used to evaluate the immunofluorescence of pDNA-PKcs after CTDSP1 knockdown with and without SN-38 exposure in cell lines HCT116 and 12-G10.

RESULTS

Inhibitor Experiment:

Western Blot Data

CPT resistant HCT-15-4E7 and sensitive HCT116 12-G10 cell lines were treated with Rabeprazole, an inhibitor of CTDSP1. We hypothesized when both SN-38 incubated cell lines were treated with Rabeprazole, CTDSP1 would be inhibited and unable to remove the phosphate from DNA-PKcs. This would result in greater phosphorylation of DNA-PKcs post Rabeprazole treatment. We also hypothesized greater phosphorylation of DNA-PKcs would be observed in HCT-15 resistant cell lines. Figure 9 shows when concentrations of Rabeprazole are increased, phosphorylation of DNA-PKcs is increased in both resistant and sensitive cell lines. The greatest amount of phosphorylated DNA-PKcs is observed in Lane 3, which represents resistant cell line HCT-15 with exposure to 10μM Rabeprazole. Figure 9 shows cells treated with greater concentrations of Rabeprazole produced darker, more prominent bands at the molecular mark phosphorylated DNA-PKCS is expected to be.

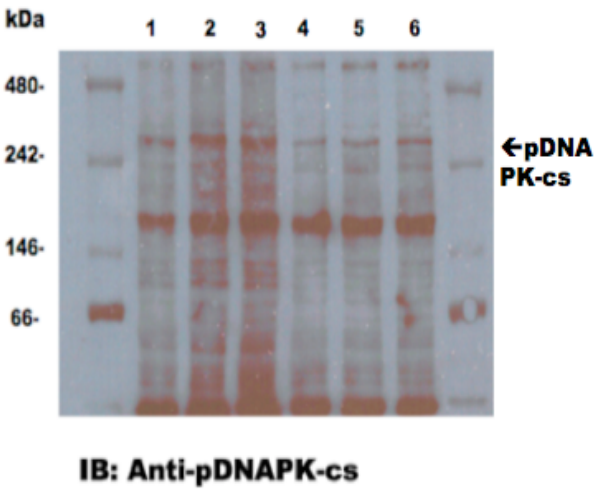

Figure 9:
Phosphorylation of DNA-PKCS in cells is enhanced after CTDSP1 inhibition with Rabeprazole: CPT-treated 4E7-HCT15 (lanes 1-3) and HCT116-12-G10 cell lysates (lanes 4-6) were analyzed by immunoblot analysis with anti-DNA-PKcs. Both lanes 1-3 and lanes 4-6 of represent cells exposed to 0μM, 5μM, and 10μM concentrations of Rabeprazole respectively. The band generated by phosphorylated DNA-PKcs appears around 460 Kda

To further explore the relationship between CTDSP1 inhibition and DNA-PKcs phosphorylation in sensitive cell lines, a western blot was conducted using cells from line HCT116-1-2G10 exposed with 0μM, 5μM, or 10μM concentrations of Rabeprazole. Additionally, only half of the cell lines were treated with SN-38 to determine whether Rabeprazole induced changes were only observable in cells incubated with SN-38

Figure 10 shows greater phosphorylation of DNA-PKcs in lanes 2 and 3 compared to lane 1, suggesting that exposure to increased amounts of Rabeprazole results in greater phosphorylation of DNA-PKcs in cell line HCT116 without SN38 treatment. In cell line HCT116-12-G10, the greatest amount of DNA-PKcs phosphorylation is observed in Lane 5, representing incubation with 5μM concentration of Rabeprazole. The greater phosphorylation of DNA-PKcs in cells observed in Lane 5, treated with 5μM Rabeprazole, in comparison to Lane 4, treated with 0μM Rabeprazole supports the role of CTDSP1 as a regulator of DNA-PKcs.

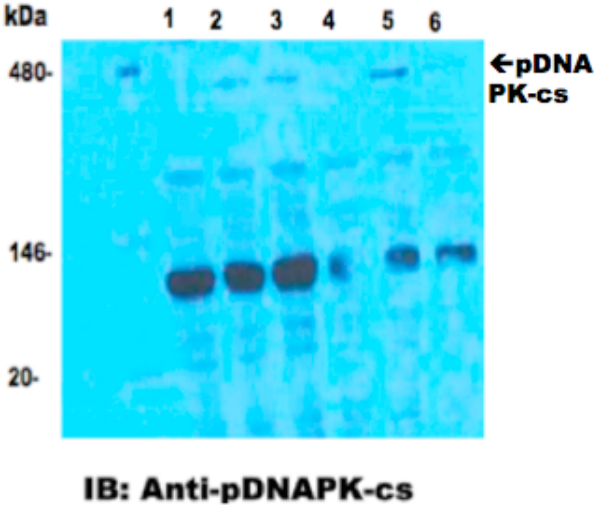

Figure 10: Phosphorylation of DNA-PKCS in CPT treated cells is enhanced after CTDSP1 inhibition with Rabeprazole: Control HCT116-12-G10 (lanes 1-3) and CPT treated HCT116-12-G10 cell lysates (lanes 4-6) were analyzed by immunoblot analysis with anti-pDNA-PKcs. Both lanes 1-3 and lanes 4-6 of represent cells exposed to 0μM, 5μM, and 10μM concentrations of Rabeprazole respectively. The band generated by phosphorylated DNA-PKcs appears around 460 Kda.

Greater phosphorylation of DNA-PKcs observed when HCT116 cell line was exposed to 5μM Rabeprazole compared to 10μM Rabeprazole observed in lane 5 and 6 of Figure 10 led to continued investigation of the effects of CTDSP1 inhibition on sensitive cell line HCT116-1-2G10 exposed to 0μM and 5μM Rabeprazole concentrations.

Both lanes 1 and 3 in Figure 11, exposed to 5μM Rabeprazole, reveal significantly greater amounts of DNA-PKcs phosphorylation in comparison to lanes 2 and 4 in Figure 11, exposed to 0μM Rabeprazole. HCT116 treated with both SN-38 and 5μM Rabeprazole in lane 3 shows the greatest amount of DNA-PKcs phosphorylation and the darkest band.

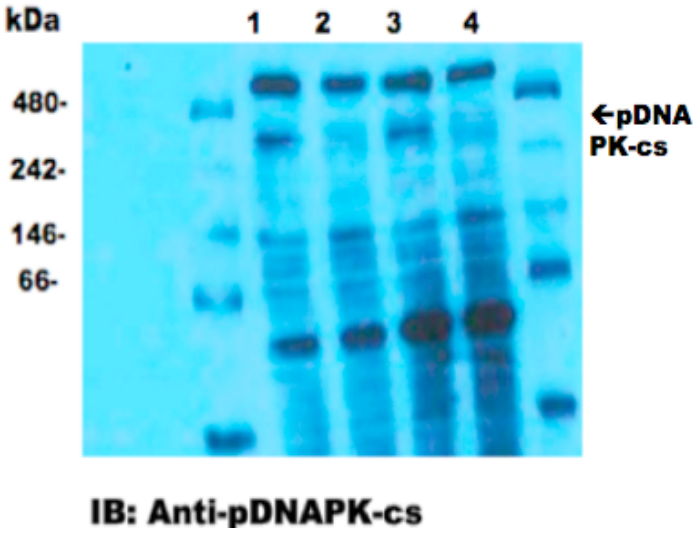

Figure 11: Phosphorylation of DNA-PKCS in CPT treated cells is enhanced after CTDSP1 inhibition with Rabeprazole: CPT treated HCT116-12-G10 (lanes 1-2) and control HCT116-12-G10 cell lysates (lanes 3-4) were analyzed by immunoblot analysis with anti-pDNA-PKcs. Both lanes 1-2 and lanes 3-4 of represent cells exposed to 5μM and 0μM of Rabeprazole respectively. The band generated by phosphorylated DNA-PKcs appears around 460 Kda.

After producing the results shown in figure 11, an experiment using the same conditions was conducted to determine whether the results were reproducible. Similar to the last experiment, the darkest band and greatest amount of DNA-PKcs phosphorylation occurred in HCT116 cells treated with both SN-38 and 5μM Rabeprazole.

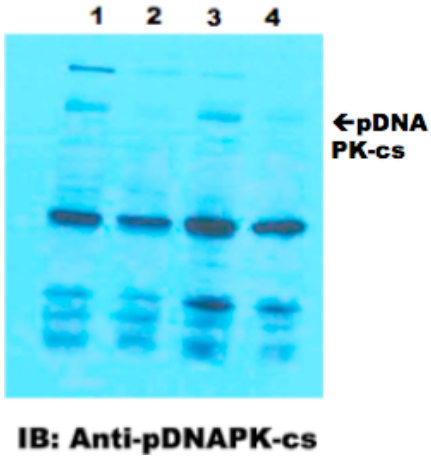

Figure 12: Phosphorylation of DNA-PKCS in CPT treated cells is enhanced after CTDSP1 inhibition with Rabeprazole: CPT treated HCT116-12-G10 (lanes 1-2) and control HCT116-1-2G10 cell lysates (lanes 3-4) were analyzed by immunoblot analysis with anti-DNA-PKcs. Both lanes 1-2 and lanes 3-4 of represent cells exposed to 5μM and 0μM of Rabeprazole respectively.

Cellular levels of topoI were also evaluated in both HCT-15-4E7 and HCT116-12-G10 cell lines after exposure to 0,5, and 10μM concentrations of Rabeprazole. In order to observe the effects of CPT on the degradation of topoisomerase, some cells from each Rabeprazole condition were exposed to SN-38. When phosphorylated, DNA-PKcs carries out a kinase function and phosphorylates topoisomerase. The phosphorylation of topoI proteins leads to ubiquitination followed by degradation of topoisomerase. Without topoisomerase, the substrate for CPT to react with is gone, and cells are more resistant to the chemotherapy treatment. CTDSP1 is a phosphatase negatively regulates DNA-PKcs by dephosphorylating and inactivating the kinase. Inactivation of DNA-PKcs prevents the phosphorylation and degradation of topoI that causes resistance.

We hypothesized that by inhibiting CTDSP1 using Rabeprazole, less topoI would be present in the cell due to greater degradation caused by constitutively active DNA-PKcs. We also hypothesized that treatment with SN-38 initiated the degradation pathway, leading to even less topoI in cells treated with both Rabeprazole and SN-38. Both

resistant cell line HCT-15-4E7 and sensitive cell line HCT116-1-2G10 were evaluated in Figure 13.

We expected to see the greatest amount of topoI degradation in the HCT15 cell line, since this cell line is resistant to CPT. Figure 13 reveals complete degradation of topoI in lanes 1 through 3 representing HCT15 cells, regardless of Rabeprazole concentration. However, sensitive HCT116 cells demonstrate greater degradation of topoI with higher concentrations of Rabeprazole. Lane 6 shows the greatest amount of degradation. This data suggests that inhibiting CTDSP1 to a greater degree enhances the degradation of topoI in sensitive cell lines.

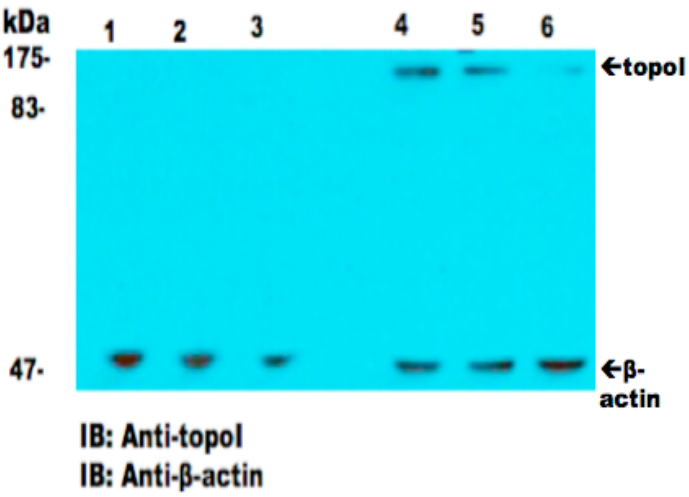

Figure 13: Greater degradation of TopoI occurs in cells after CTDSP1 inhibition with Rabeprazole: CPT-treated 4E7-HCT15 (lanes 1-3) and HCT116-12-G10 cell lysates (lanes 4-6) were analyzed by immunoblot analysis with anti-topoI and anti-β-Actin. Both lanes 1-3 and lanes 4-6 of represent cells exposed to 0μM, 5μM, and 10μM concentrations of Rabeprazole respectively.

The effects of SN-38 and Rabeprazole on the sensitive HCT116 cell line were further explored in a follow up western blot shown in Figure 14. Lane 1 produced the darkest topoI band and contained cells treated without Rabeprazole and SN-38. Fainter topoI bands were observed in the latter 2 lanes exposed to SN-38. Lane 2, treated with 5μM Rabeprazole, revealed a somewhat fainter topoI band than the band in Lane 1.

Figure 14 reveals similar results to figure 5, suggesting that treatment with SN-38 and Rabeprazole lead to lower levels of topoI.

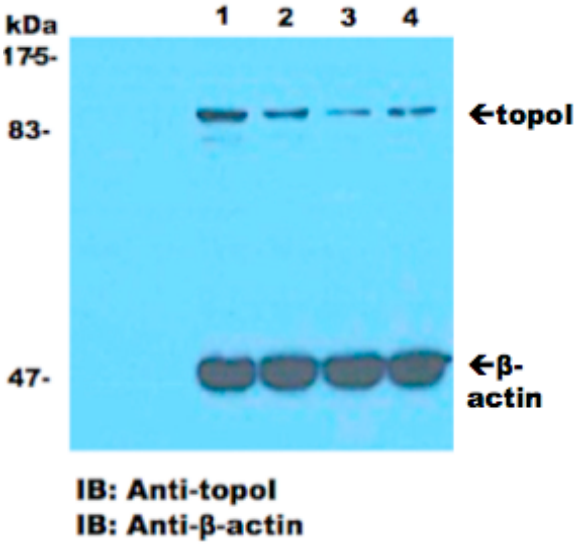

Figure 14:
Greater degradation of TopoI occurs in cells after CTDSP1 inhibition with Rabeprazole: HCT116-12-G10 (lanes 1-2) and control HCT116-12-G10 cell lysates (lanes 3-4) were analyzed by immunoblot analysis with anti-topoI and anti-β-Actin. Both lanes 1-2 and lanes 3-4 represent cells exposed to 0μM and 5μM concentrations of Rabeprazole.

***Clonogenic Assay Data*:** A clonogenic assay was conducted in order to compare the survival of HCT116 cells exposed to 10μM Rabeprazole and 0μM Rabeprazole after incubation with varying concentrations of SN-38.

Cell Counting Data: The HCT116 cells from the 0μM Rabeprazole control condition were first counted.

Table 21: Amount of Control HCT116 cells exposed to varying concentrations of SN-38

SN38 concentration	Cells # Well 1	Cell # Well 2	Cell # Well 3
0nM	45	41	43
0.5nM	27	24	34
1.0nM	18	0	15
2.5nM	10	8	11
5.0nM	1	1	0
7.5nM	0	1	0

The amount of HCT116 cells exposed to 0nM SN-38 in each well were then converted to a percentage shown in the table below.

Table 22: Percentage of control HCT116 cells remaining after exposure to varying concentrations of SN-38

0nM SN-38 Concentration	Percentage of Cells (PE) (cell colony #/50*100)
Well 1 45/(50*100)	90
Well 2 41/(50*100)	82
Well 3 43/ (50*100)	86
PE Average	86
50*PE Average	4300

The surviving fraction for HCT116 cells exposed to 0μM Rabeprazole was calculated for each SN-38 condition.

Surviving Fraction Calculation: Cell colony number in well/50*PE Average
The PE Average=86
86*50=4300

Example: Well 1 Surviving fraction
45/ 4300 = 0.010465116

Table 23: Surviving Fraction of control HCT116 cells after exposure to varying concentrations of SN-38

	Well 1	Well 2	Well 3	SF Average
Surviving Fraction 0nM wells	0.010465116	0.009534884	0.01	0.01
Surviving Fraction 0.5 nM wells	0.00627907	0.005581395	0.007906977	0.006589147
Surviving Fraction 1.0 nM wells	0.004186047	0	0.003488372	0.003837209
Surviving Fraction 2.5	0.002325581	0.001860465	0.00255814	0.002248062

nM wells				
Surviving Fraction 5.0 nM wells	0.000232558	0.000232558	0	0.000155039
Surviving Fraction 7.5 nM wells	0	0.000232558	0	7.75194E-05

The HCT116-1-2G10 cells from the 10μM Rabeprazole control condition were then counted.

Table 24: Amount of 10μM Rabeprazole incubated HCT116-1-2G10 cells exposed to varying concentrations of SN-38

SN38 concentration	Cell # Well 1	Cell # Well 2	Cell #Well 3
0nM	39	46	0
0.5nM	45	0	48
1.0nM	41	33	41
2.5nM	0	16	28
5.0nM	5	7	3
7.5nM	4	3	3

The amount of HCT116 cells exposed to 0nM SN-38 in each well were then converted to a percentage shown in the table below.

Table 25: Percentage of 10μM Rabeprazole incubated HCT116-1-2G10 cells exposed to varying concentrations of SN38

0nM SN-38 Concentration	Percentage of Cells (PE) (cell colony #/50*100)
Well 1 39/(50*100)	78
Well 2 46/(50*100)	92
Well 3	0

0/ (50*100)	
PE Average	85
50*PE Average	4250

The surviving fraction for HCT116 cells exposed to 0μM Rabeprazole was calculated for each SN-38 condition.

Table 26: Surviving Fraction of 10μM Rabeprazole incubated HCT116-1-2G10 cells exposed to varying concentrations of SN-38

	Well 1	Well 2	Well 3	SF Average
Surviving Fraction 0nM wells	0.009176471	0.010823529	0	0.01
Surviving Fraction 0.5 nM wells	0.010588235	0	0.011294118	0.010941176
Surviving Fraction 1.0 nM wells	0.009647059	0.007764706	0.009647059	0.009019608
Surviving Fraction 2.5 nM wells	0	0.003764706	0.006588235	0.005176471
Surviving Fraction 5.0 nM wells	0.001176471	0.001647059	0.000705882	0.001176471
Surviving Fraction 7.5 nM wells	0.000941176	0.000705882	0.000705882	0.000784314

We compared the average survival fraction of HCT116 cells exposed to 0μM and 10μM concentrations of Rabeprazole after SN-38 treatment in order to determine the influence of Rabeprazole on HCT116 cell survival after exposure to SN-38. Table 27 shows the survival rate of HCT116 cells treated with 10μM Rabeprazole increases in

comparison to HCT116 cells treated with 0μM Rabeprazole with increasing concentrations of SN-38.

Table 27: Average Survival Fraction Comparison between 0μM Rabeprazole incubated HCT116-1-2G10 cells and 10μM Rabeprazole incubated HCT116 cells exposed to SN-38

SN-38 exposure concentrations	Control HCT116	10μM Rabeprazole treated HCT116
0nM	0.01	0.019019608
0.5nM	0.006589147	0.010941176
1.0nM	0.003837209	0.009019608
2.5nM	0.002248062	0.005176471
5.0nM	0.000155039	0.001176471
7.5nM	7.75194E-05	0.000784314

Table 28 reveals the standard deviations between wells evaluating similar conditions. A large standard deviation margin is notable at the 2.5nM SN-38 concentration, suggesting this data may be less reliable than the other values. The remaining values have smaller error margins.

Table 28: Standard Deviation Survival Fraction Comparison between control HCT116 cells and 10μM Rabeprazole incubated HCT116-1-2G10 cells exposed to SN-38

SN-38 exposure concentrations	Control HCT116	10μM Rabeprazole treated HCT116
0nM	0.000465116	0.001164646
0.5nM	0.001193396	0.000499134
1.0nM	0.00049333	0.001086777

2.5nM	0.000355238	0.001996537
5.0nM	0.000134268	0.000470588
7.5nM	0.000134268	0.000135847

Below, Figure 15 graphically visualizes the data presented in Tables 27 and 28. The blue line represents the control condition of HCT116 cells exposed to 0µM Rabeprazole. The red line signifies the HCT116 cells exposed to 10µM Rabeprazole. The graph demonstrates no observable difference between the control and Rabeprazole treatment conditions when exposed to 0nM SN-38. Additionally, the graph suggests that Rabeprazole treated HCT116 cells have a greater survival fraction when exposed to SN38 compared to control HCT116 cells. The survival fraction of both treated and untreated HCT116 cells is lowest at 5.0 and 7.5 nM concentrations of SN-38. Although the survival fraction of Rabeprazole treated HCT116 cells is greater than the controls after SN-38 treatment, the survival of treated HCT116 cells is greatest at the lowest 0 and 0.5 nM concentrations of SN-38.

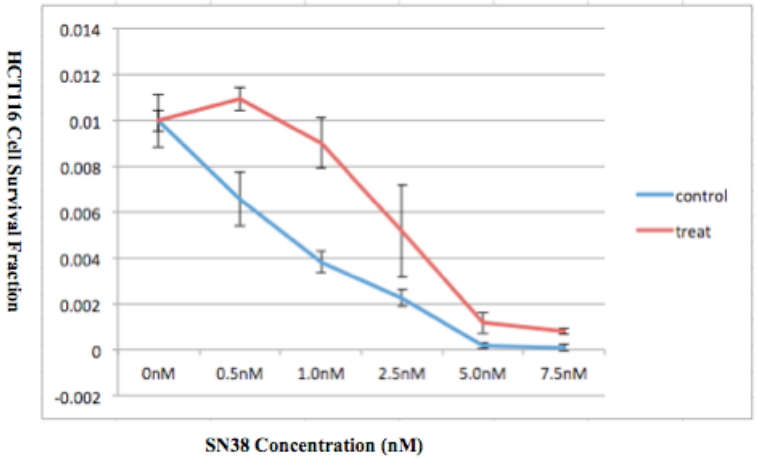

Figure 15: Survival Fraction of HCT116 cells treated with 0µM and 10µM concentrations of Rabeprazole at different SN-38 concentrations

***Immunofluorescent Staining of pDNA-PKcs Results*:**

The effects of Rabeprazole on the amount of phosphorylated DNA-PKcs present in cell line HCT116-1-2G10 was investigated using immunofluorescent staining. HCT116 cells exposed to both 0μM and 10μM concentrations of Rabeprazole were treated with anti pDNA-PKcs primary antibody and α-Rb-Green secondary antibody. If there were greater levels of pDNA-PKcs in the cells, then the cells would stain a fluorescent green. As a control, all HCT116 cells were also stained with DAPI (4',6-diamidino-2-phenylindole), a fluorescent blue stain that binds strongly to A-T rich regions in DNA. Therefore, the DAPI stain shows up in the nuclear region of HCT116 cells treated both 0μM and 10μM concentrations of Rabeprazole. All microscope photograph comparisons were taken at the same location on the slide. We hypothesized greater levels of pDNA-PKcs would be present in the HCT116 cells treated with 10μM Rabeprazole in comparison to cells exposed to 0μM Rabeprazole. Rabeprazole inhibits CTDSP1, which prevents the dephosphorylation of DNA-PKcs. Phosphorylated DNA-PK is the active form of the kinase responsible for phosphorylating and initiating the degradation pathway of topoI. We expected to see a greater amount of green fluorescence in the HCT116 cell line treated with 10μM Rabeprazole compared to the 0μM Rabeprazole HCT116 cells. Additionally, we expected to see no difference in the DAPI stain, blue immunofluorescence, between the HCT116 cell groups. Figure 16A shows the pDNA-PKcs green staining of HCT116 cells exposed to 0μM Rabeprazole. Figure 16B shows the DAPI staining of HCT116 cells exposed to 0μM Rabeprazole. The photographs below exhibit the exact same region of the microscope set to different stain

settings. These results suggest that under the control Rabeprazole condition, almost no DNA-PKcs is phosphorylated in any HCT116 cells.

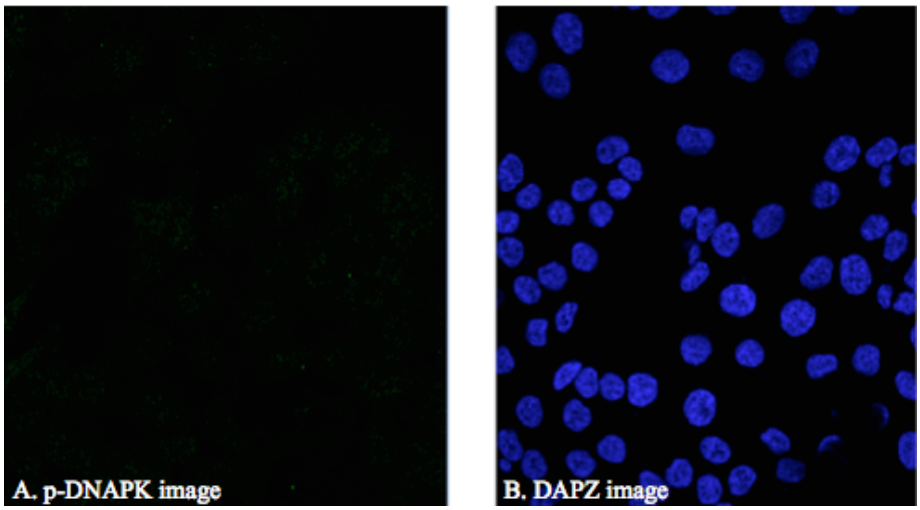

Figure 16A: α-Rb-Green Immunofluorescent stain detecting phosphorylated DNA-PKCS in HCT116 cells treated with 0μM Rabeprazole: HCT116 cells were treated with the primary antibody anti pDNA-PKCS and secondary antibody α-Rb-Green. A small green fluorescent speck of pDNA-PKCS was revealed under the microscope. **16B: DAPI blue Immunofluorescent stain detecting A-T rich regions in DNA in HCT116 cells treated with 0μM Rabeprazole**

The photographs below exhibit the exact same region of the microscope set to different stain settings. These microscope photographs further suggest that under the control Rabeprazole condition, there is little DNA-PKcs phosphorylation in HCT116 cells.

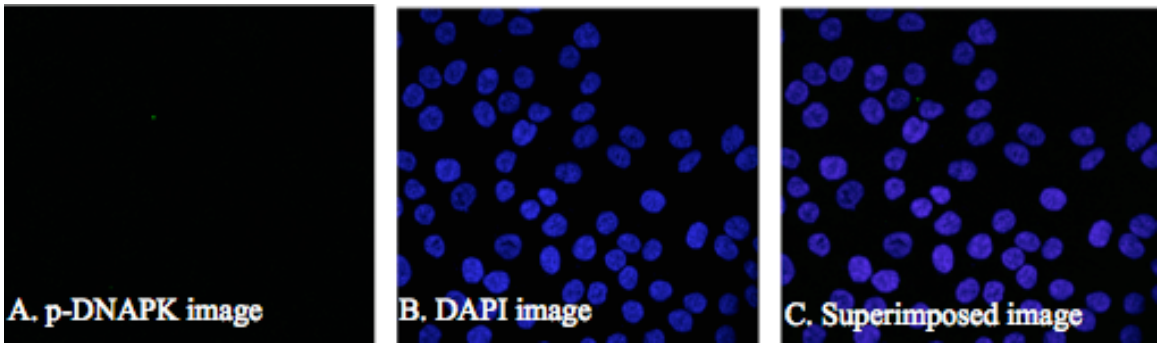

Figure 17A: α-Rb-Green Immunofluorescent stain detecting phosphorylated DNA-PKCS in HCT116 cells treated with 0μM Rabeprazole. HCT116 cells were treated with the primary antibody anti pDNA-PKCS and secondary antibody α-Rb-Green. A small green fluorescent speck of pDNA-PKCS was revealed under the microscope. **17B: DAPI blue Immunofluorescent stain detecting A-T rich regions in DNA in HCT116 cells treated with 0μM Rabeprazole**
17C: α-Rb-Green and DAPI blue Immunofluorescent stain superimposed on one another in HCT116 cells treated with 0μM Rabeprazole. This figure demonstrates the images in 8A and 8B are taken from the same frame.

Figure 18A shows the pDNA-PKcs green staining of HCT116 cells exposed to 10μM Rabeprazole. Figure 18B shows the DAPI staining of HCT116 cells exposed to 10μM Rabeprazole. Figure 18C reveals the pDNA-PKcs green stain superimposed upon the DAPI stain of HCT116 cells. The photographs below exhibit the exact same region of the microscope set to different stain settings. These results suggest that under the 10μM Rabeprazole condition, a greater amount of DNA-PKcs is phosphorylated in comparison to the control condition.

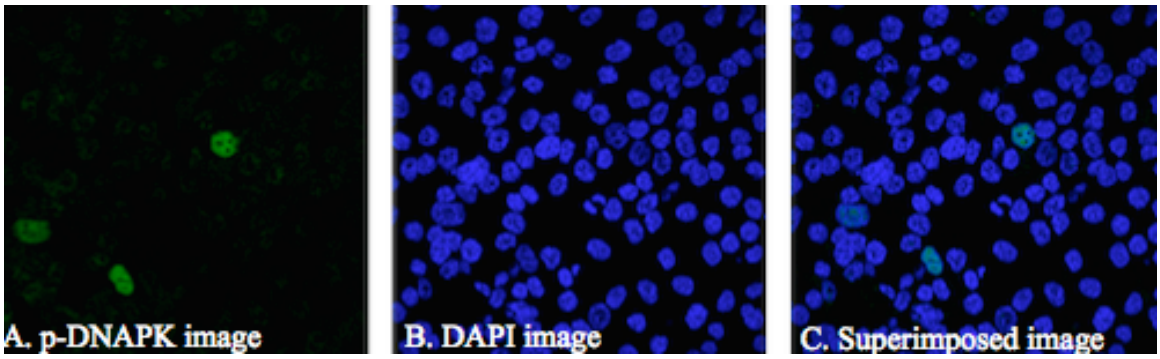

Figure 18A: α-Rb-Green Immunofluorescent stain detecting phosphorylated DNA-PKcs in HCT116 cells treated with 10μM Rabeprazole
18B: DAPI blue Immunofluorescent stain detecting A-T rich regions in DNA in HCT116 cells treated with 10μM Rabeprazole
18C: α-Rb-Green and DAPI blue Immunofluorescent stain superimposed on one another in HCT116 cells treated with 10μM Rabeprazole

Figure 19 shows a zoomed in version of the images displayed in Figure 10.

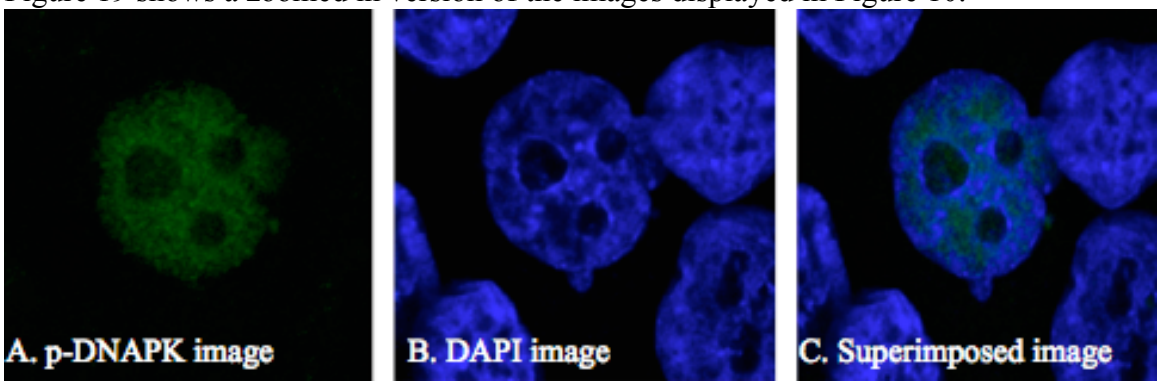

Figure 19A: α-Rb-Green Immunofluorescent stain detecting phosphorylated DNA-PKcs in HCT116 cells treated with 10μM Rabeprazole
19B: DAPI blue immunofluorescent stain
19C: α-Rb-Green and DAPI blue Immunofluorescent stain superimposed on one another in HCT116 cells treated with 10μM Rabeprazole

Image of topoI-EGFP Results:

The effects of Rabeprazole on the amount of topoI present in cell line HCT116 was investigated by tagging EGFP to topoI. Figure 20 shows the EGFP fluorescence of HCT116 cells were incubated with 0, 5, and 10μM concentrations of Rabeprazole.

Inhibition of CTDSP1 results in greater DNA-PKcs phosphorylation and topoI degradation. We hypothesized that HCT116 cells exposed to greater concentrations of Rabeprazole, a CTDSP1 inhibitor, would have lower levels of topoI and present a decreased amount of EGFP fluorescence. Figure 20 reveals the greatest amount of topoI-EGFP fluorescence in cells incubated with 0μM Rabeprazole and the least amount of topoI-EGFP fluorescence in cells incubated with 10μM Rabeprazole. Less topoI-EGFP fluorescence with increasing amounts of Rabeprazole suggests that inhibition of CTDSP1 enhances topoI degradation in HCT116 cells.

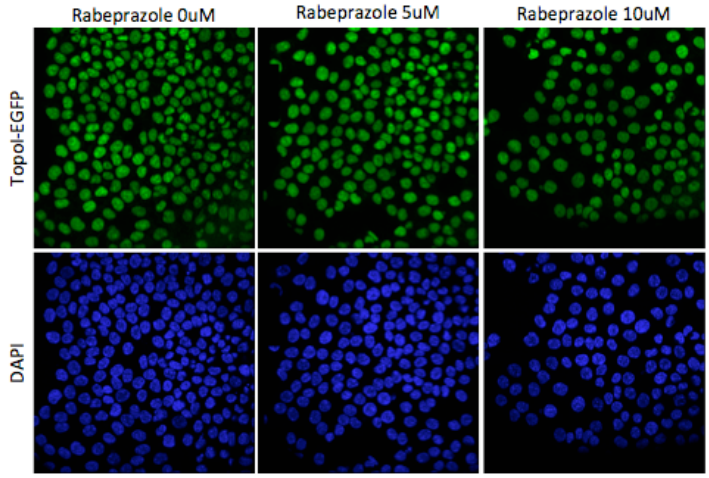

Figure 20: Visualization of TopoI EGFP in HCT116-1-2G10 cells treated with 0μM, 5μM and10μM concentrations of Rabeprazole

CTDSP1 Knockdown Experiments

Western Blot Data:

The results of the inhibitor experiments suggest an influence of CTDSP1 on the topoI degradation pathway in sensitive cell lines. We decided to see if similar findings could be produced in sensitive cell lines HCT116 and 12-G10 after knocking down

CTDSP1 completely using siRNA. We expected to observe greater DNA-PKcs phosphorylation in cell lines in the CTDSP1 knock down condition, for CTDSP1 is the phosphatase that removes the phosphate from DNA-PKcs. We also hypothesized that the magnitude of DNA-PKcs phosphorylation would be enhanced in cell lines exposed to SN-38, which in previous experiments appeared to jumpstart the degradation pathway. Lane 1 revealed no band for DNA-PKcs phosphorylation and contained cell line HCT116 with functional CTDSP1 and without exposure to SN-38. In contrast, lane 2, also containing functional CTDSP1 did produce a pDNA-PKcs band. The only difference between lanes 1 and 2 was incubation of HCT116 cells with SN-38 in lane 2. This suggests that SN-38 treatment contributes to greater phosphorylation of DNA-PKcs even when CTDSP1 is functional. Lanes 5 and 6 demonstrate the pDNA-PKcs band produced by cell line 12-G10 with functional CTDSP1. Lane 6, the condition with SN-38 treatment, shows a darker band than lane 5. This evidence further supports the role of SN-38 as a contributing factor to greater DNA-PKcs phosphorylation. The light band produced in Lane 8, demonstrating the CTDSP1 knockdown after incubation with SN-38 deviates from our expectations. In this situation, we would expect a darker band since there is no phosphatase present to dephosphorylate DNA-PK.

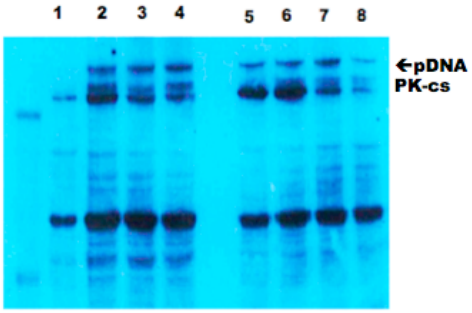

Figure 21:
Phosphorylation of DNA-PKCS in cells is enhanced both after incubation with CPT: HCT116 (lanes 1-4) and HCT116-12-G10 (lanes 5-8) cell lysates were analyzed by immunoblot analysis with anti-pDNA-PKcs. The band generated by phosphorylated DNA-PKcs appears around 460 Kda. Lysates in lanes 2,4,6, and 8 were treated with CPT. Lanes 3,4,7,and 8 demonstrate CTDSP1 knock down conditions.

Because of the discrepancy seen in results from the previous pDNA-PKCS experiment, we decided to conduct an additional western blot shown in Figure 22 to examine pDNA-PKCS levels after CTDSP1 knockdown and SN-38 treatment. While the control conditions shown in lanes 1 and 2 looked relatively similar, there were differences observed between the CTDSP1 knock down conditions observed in lanes 3 and 4. A fainter band is observed in lane 3, which represents the CTDSP1 knockdown without SN-38 treatment. The darkest band is shown in lane 4, which represents the CTDSP1 knockdown and SN-38 incubation. These results further suggest the enhanced effect on DNA-PKcs phosphorylation produced when both CTDSP1 is knocked down and cells are treated with SN-38. Lanes 5 and 6, containing cell line 12-G10 in the control condition, produced bands that demonstrate differences in DNA-PKcs phosphorylation after exposure to SN-38. The pDNA-PKcs band in Lane 6 is darker than the one produced in lane 5. These results also support the idea that greater phosphorylation of DNA-PKcs occurs in cells after exposure to SN-38. Lanes 7 and 8 showed bands produced by cell line 12-G10 after CTDSP1 knockdown. The contrast between these bands is greater than the contrast between lanes 5 and 6, suggesting treatment with SN-38 has more pronounced effects on cells lacking functional CTDSP1 relative to controls. Lane 8 produced the darkest band for the 12-G10 cell line, meaning the greatest phosphorylation of DNA-PKcs occurred in cells lacking CTDSP1 and incubated with SN-38. Unlike the previous blot, the protein concentrations in Figure 22 appear more consistent between lanes.

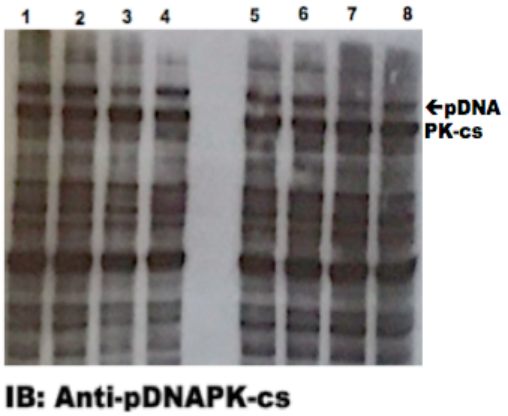

Figure 22: Phosphorylation of DNA-PKCS in cells is enhanced both after CTDSP1 knock down and incubation with CPT: HCT116 (lanes 1-4) and HCT116-12-G10 (lanes 5-8) cell lysates were analyzed by immunoblot analysis with anti-DNA-PKcs. The band generated by phosphorylated DNA-PKcs appears around 460 Kda. Lysates in lanes 2,4,6, and 8 were treated with CPT. Lanes 3,4,7,and 8 demonstrate CTDSP1 knock down conditions.

After knocking down CTDSP1 in cell lines HCT116 and 12-G10, we also demonstrated the amount of topoI present in the cells after treating with and without SN-38 in Figure 23. We expected CTDSP1 knockdown cells to lead to greater DNA-PKcs phosphorylation and subsequent topoI degradation. Additionally, we suspected treatment with SN-38 would accelerate the topoI degradation process. No notable significant differences were noticed in bands produced by the HCT116 cell line. The faintest band was produced in Lane 8, which represents cell line 12-G10 with both CTDSP1 knock down and SN-38 exposure. Lane 8 produced a significantly darker actin band than the other lanes, suggesting that a greater concentration of protein was present in this condition compared to the other bands. However, even with extra protein, lane 8 still produced a lighter band.

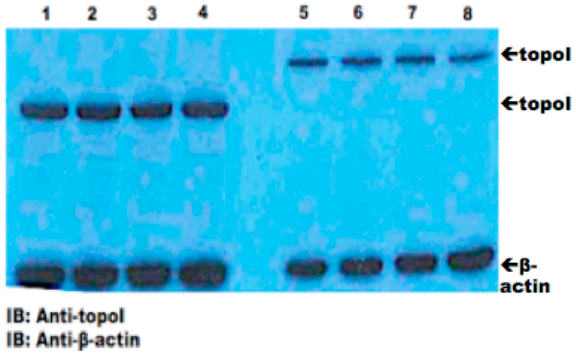

Figure 23:
Greater degradation of TopoI occurs in cells after CTDSP1 knockdown and CPT exposure: HCT116 (lanes 1-4) and HCT116-12-G10 (lanes 5-8) cell lysates were analyzed by immunoblot analysis with anti-topoI and anti-β-Actin. Lysates in lanes 2,4,6, and 8 were treated with CPT. Lanes 3,4,7,and 8 demonstrate CTDSP1 knock down conditions. The top and bottom bands show levels of topoI and actin respectively.

For the previous results to be valid, we needed to confirm the knockdown of CTDSP1 was successful. We conducted the western blot shown in Figure 24 to test for the presence of CTDSP1. The dark bands produced in lanes 1,2, 5, and 6 show the presence of CTDSP1 protein. The fainter bands are produced in lanes representing the CTDSP1 knockdown condition for both cell lines demonstrate that the knockdown of CTDSP1 was successful. These results also indicate that the experiments examining pDNA-PKcs and topoI shown above are portraying the contrast between CTDSP1 knockdown and normal control cells.

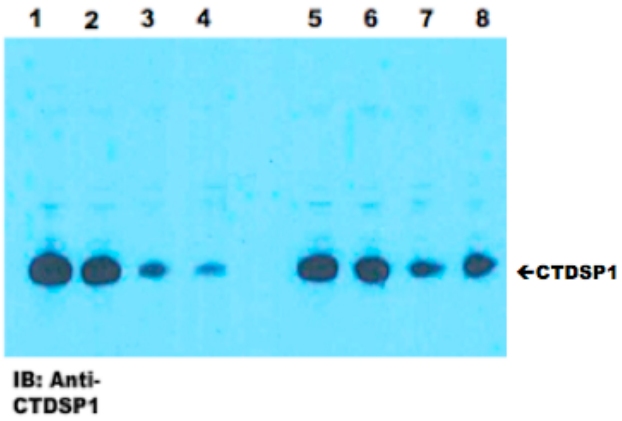

Figure 24 Confirmation of CTDSP1 knockdown: HCT116 (lanes 1-4) and HCT116-12-G10 (lanes 5-8) cell lysates were analyzed by immunoblot analysis with anti-CTDSP1. Lanes 3,4,7,and 8 demonstrate CTDSP1 knock down conditions. CTDSP1 is an approximately 31.2 Kda protein

After examining the effects of knocking down CTDSP1 on both cell lines HCT116 and 12-G10, the results for cell line HCT116 were not conclusive. In order to provide further evidence for the role of CTDSP1 in the topoI degradation pathway in cell line HCT116, we conducted an additional Western Blot. Both lanes 1 and 2 in Figure 25 produced lighter topoI bands in comparison to lanes 3 and 4. Similar to previous blots, these results suggest knocking down CTDSP1 leads to greater degradation of topoI. The inability of CTDSP1 knockdown cells to dephosphorylate DNA-PKcs and regulate

phosphorylation of topoI accelerates the topoI degradation pathway. We also expected to see fainter TopoI bands in SN-38 treated conditions. Regarding the control conditions, SN-38 treated cells in lane 3 appears somewhat lighter than lane 4. Additionally, SN-38 treated cells in lane 1 produced a fainter band than lane 1. These results provide further evidence that in addition to CTDSP1 knockdown, treatment with SN-38 augments the topoI degradation pathway. The magnitude of the actin bands is similar in each lane, reflecting that equal concentrations of cell proteins were used in each experimental condition.

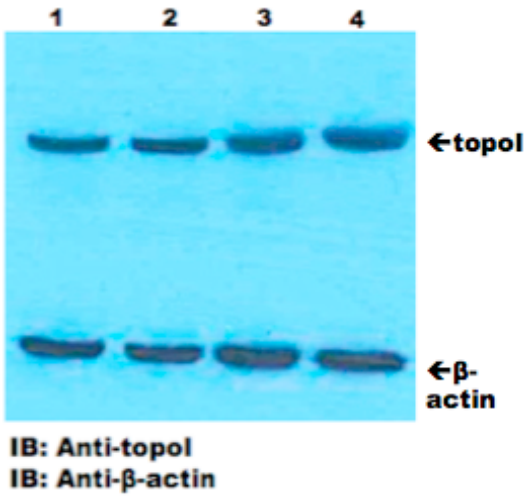

Figure 25: Greater degradation of TopoI occurs in cells after CTDSP1 knockdown and CPT exposure: HCT116 (lanes 1-4) were analyzed by immunoblot analysis with anti-topoI and anti-β-Actin. Lysates in lanes 1 and 3 were treated with CPT. Lanes 1 and 2 demonstrate CTDSP1 knock down conditions. The top and bottom bands show levels of topoI and actin respectively.

In order to confirm that knockdown successfully occurred in the siRNA condition of the previous experiment, we ran an additional western blot to check for the presence of CTDSP1. The production of lighter bands by the latter two lanes in Figure 26 suggests that the knockdown of CTDSP1 was successful in these conditions. Therefore, the results generated in experiments using these cell lines are reflective of the stated experimental conditions.

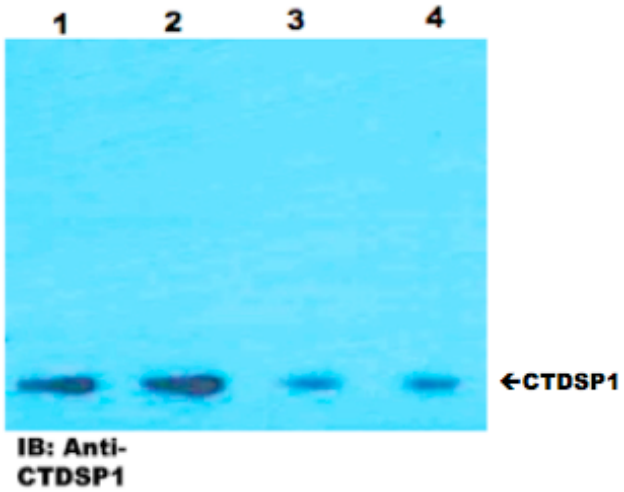

Figure 26: Confirmation of CTDSP1 knockdown: HCT116 (lanes 1-4) cell lysates were analyzed by immunoblot analysis with anti-CTDSP1. Lanes 3 and 4 demonstrate CTDSP1 knock down conditions. CTDSP1 is an approximately 31.2 Kda protein.

***Immunofluorescent Staining of pDNA-PKcs Results*:**

We used immunofluorescent staining to determine whether greater amounts of pDNA-PKcs would be observed after knocking down CTDSP1 in HCT116 cells. Figure 27 shows the amount of pDNA-PKcs after CTDSP1 knockdown with and without SN-38 treatment. Additionally, figure 27 demonstrates the effects of SN-38 on pDNA-PKcs levels in control conditions as well. Similar to the previous immunofluorescence experiments, DAPI was used to confirm the presence of cells in each condition by staining the nuclear region of cells. The greatest green immunofluorescence is observed in the CTDSP1 knockdown condition exposed to SN-38. While null-CTDSP1 cells produced moderate levels of immunofluorescence, the effects on pDNA-PKcs were intensified when HCT116 cells experienced CTDSP1 knockdown and SN-38 treatment. Control cells without SN-38 incubation showed no immunofluorescence, and HCT116 cells treated with SN-38 showed very small amounts of DNA-PKcs phosphorylation. These results suggest that CTDSP1 is involved in CPT resistance via regulation of DNA-PKcs phosphorylation. In addition, these results show SN-38 treatment increases the rate

of DNA-PKcs phosphorylation in both control and CTDSP1 knockdown cells. However, the impact of SN-38 is greatest in cells without CTDSP1.

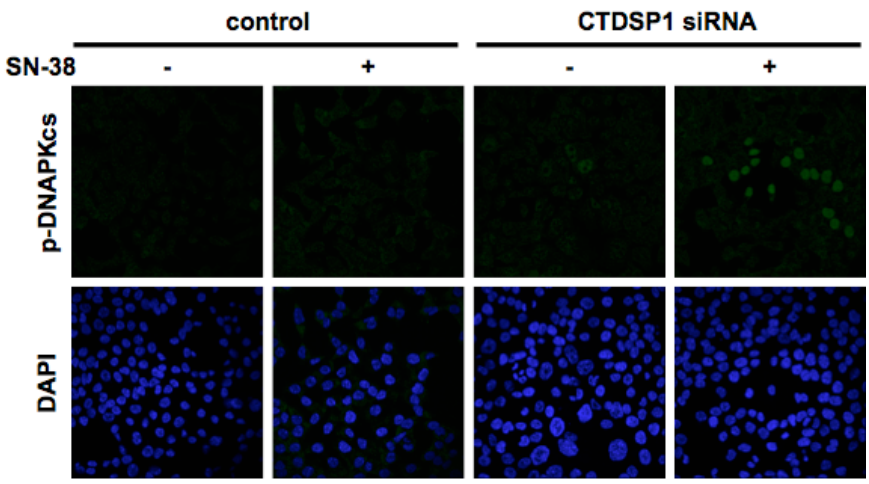

Figure 27: α-Rb-Green Immunofluorescent stain detecting phosphorylated DNA-PKcs in both control and CTDSP1 knockdown HCT116 cells

Discussion

In previous colorectal cancer clinical cases, certain cell lines have proven more resistant to CPT chemotherapy treatment than others (Ando et al. 2017). Generating a better understanding of the pathway that leads to cellular resistance to CPT may allow physicians to identify whether the treatment will be effective in different patients. If cellular resistance to CPT can be recognized in a patient before treatment, then patients can be provided with an alternative chemotherapy option. In order to establish biomarkers of cellular resistance, we examined the topoI degradation pathway involved in CPT resistance. The Bharti lab has demonstrated that DNA-PKcs dependent phosphorylation of topoI is critical for the CPT induced degradation of topoI. High basal levels of topoI s10 phosphorylation ensure CPT resistance in caner cells. We asked if DNA-PKcs is regulated by a phosphatase that maintains higher DNA-PKcs activity and high basal level of topoI to impart CPT resistance. The Bharti lab did an siRNA library

screen of all nuclear phosphatase to identify the upstream regulator of DNA-PK and have identified PTEN and CTDSP1 as two potential regulators of DNA-PK activity. In this study we looked at the role of the phosphatase CTDSP1 in the regulation of DNA-PKcs, the topoI degradation pathway, and whether CTDSP1 influenced cell survival after CPT exposure.

CTDSP1 Inhibition

One of the functions of CTDSP1 is to dephosphorylate the kinase DNA-PKcs (Ando et al. 2017). This phosphate removal renders DNA-PKcs inactivated and unable to phosphorylate topoI. Phosphorylation of topoI initiates ubiquitination followed by degradation of topoI. If topoI is degraded, CPT has no substrate to interact with and is unable to destroy cells via topoI inhibition (Ando et al. 2017).

DNA-PKcs phosphorylation in cell lines HCT116 and HCT15

In the first series of experiments, the phosphorylation of DNA-PKcs in two cell lines was evaluated using western blots after exposure to CPT and 0μM, 5μM, and 10μM concentrations of Rabeprazole. When inhibited, CTDSP1 is unable to remove the phosphate from DNA-PKcs, so we expected to observe greater DNA-PKcs phosphorylation in cells incubated with larger concentrations of Rabeprazole. The cell lines used included sensitive line HCT116 and resistant line HCT15. When treated with CPT, cell line HCT116 is more responsive than HCT15, resulting in greater cell death from the HCT116 cell line (Goldwasser et al.1994). The resistance of cell line HCT15 is due to enhanced topoI degradation in comparison to cell line HCT116 after treatment with CPT.

We wondered if differences between the cell lines would also manifest in DNA-PKcs phosphorylation when both cell lines experienced CTDSP1 inhibition. After treating cells with 0μM, 5μM, and 10μM concentrations of Rabeprazole for 4 days and CPT for 1 hour, we used a western blot to detect the phosphorylation of DNA-PKcs. The higher DNA-PKcs phosphorylation was observed in cell line HCT15 treated with both CPT and 10μM Rabeprazole. Within the HCT116 cell line conditions, significantly higher DNA-PKcs phosphorylation was also exhibited in the 10μM Rabeprazole condition. When comparing the two cell lines, the HCT15 cell line produced the most prominent bands indicating DNA-PKcs phosphorylation. These results show that inhibiting CTDSP1 influences both sensitive and resistant cell lines and results in greater DNA-PKcs phosphorylation. The more notable influence of CTDSP1 inhibition in the resistant cell line suggests that these cells may already have less functional CTDSP1 or some other factor contributing to increased phosphorylation of DNA-PKcs. Additionally, these cells may have higher basal levels of DNA-PKcs phosphorylation than sensitive cell lines. Larger amounts of phosphorylated DNA-PKCS in basal conditions may be a potential indicator of cellular resistance to CPT. Furthermore, enhanced levels of phosphorylated DNA-PKcs caused by inhibition of CTDSP1 in the sensitive HCT116 cell line may lead to greater resistance of this strain to CPT.

DNA-PKcs phosphorylation in cell line HCT116

We further explored the effects of CTDSP1 inhibition on the sensitive HCT116 cell line by conducting a western blot measuring phosphorylated DNA-PKcs after cellular exposure to 0μM, 5μM, and 10μM concentrations of Rabeprazole. Previous

results suggested Rabeprazole treatment leads to increased DNA-PKcs phosphorylation and initiation of the topoI degradation pathway in cell line HCT116 after CPT treatment. We wanted to see if Rabeprazole would also present cellular effects when cells were not exposed to CPT. To determine whether the effects of Rabeprazole were enhanced by CPT treatment, we used both HCT116 cells treated with and without CPT. Western blot analysis revealed the greatest amount of DNA-PKcs phosphorylation to take place in the CPT treated 5μM Rabeprazole condition. We expected to see the stronger band in the CPT treated 10μM Rabeprazole condition, but this band was lighter than that of the CPT treated 10μM Rabeprazole condition. This result may be due to a lower concentration of protein placed into this well, for the actin control band was also smaller at the bottom of the blot. However, we also speculated whether 10μM Rabeprazole was a toxic dose amount that resulted in cell death.

HCT116 cells not exposed to CPT also demonstrated stronger signal in both the 5μM and 10μM Rabeprazole conditions. The bands were not as pronounced as the band produced by cells in the 5μM Rabeprazole and CPT treated condition. The greater DNA-PKcs phosphorylation observed in CPT treated compared to non-treated cells proposes a role of CPT in initiating the cellular resistance topoI degradation pathway. Cellular resistance to CPT appears to be two pronged and influenced not only by the presence of Rabeprazole, but also by exposure to CPT.

Because DNA-PKcs exhibited the greatest amount of phosphorylation in the CPT treated 5μM Rabeprazole condition in the last experiment, we conducted another western blot only examining the effects of 0μM and 5μM concentrations of Rabeprazole on

HCT116 cells treated with and without CPT. The greatest phosphorylation of DNA-PKcs occurred in the 5μM CPT treated condition producing the darkest band in the Western blot. In the cells without CPT exposure, the DNA-PKcs phosphorylation was greater in the 5μM condition compared to the 0μM condition. However, the DNA-PKcs phosphorylation of the 5μM Rabeprazole cells treated without CPT was less than the DNA-PKcs phosphorylation of 5μM Rabeprazole cells treated with CPT. These results further suggest the additive effects of Rabeprazole and CPT treatment combined on DNA-PKcs phosphorylation and greater cellular resistance to CPT.

TopoI levels in cell lines HCT116 and HCT15

The previous western blots examining DNA-PKcs phosphorylation revealed greater DNA-PKcs phosphorylation after cells were treated with both CPT and Rabeprazole. Once phosphorylated, the function of DNA-PKcs is to phosphorylate topoI, marking the protein for ubiquitination followed by degradation. Along with the greater phosphorylation of DNA-PKcs observed, we also expected to see greater topoI degradation after inhibiting CTDSP1. We first produced a western blot evaluating topoI levels in resistant cell line HCT15 and sensitive cell line HCT116 after treatment with CPT and 0μM, 5μM, and 10μM concentrations of Rabeprazole. Unlike cell line HCT116, the HCT15 cell line did not produce a topoI band in any of the Rabeprazole conditions. Even when CTDSP1 was not inhibited, cell line HCT15 did not reveal the presence of topoI after treatment with CPT. These results support the role of accelerated topoI degradation as a contributor to the resistant nature of cell line HCT15 to CPT. In contrast to HCT15 cells, the HCT116 cell line produced a topoI band in each Rabeprazole

treatment condition. The darkest topoI band was shown in the 0μM Rabeprazole condition and the faintest topoI band was observed in the 10μM Rabeprazole condition. Greater CTDSP1 inhibition leads to augmented topoI degradation in the sensitive HCT116 cell line. From a mechanistic perspective, CTDSP1 appears to inhibit the dephosphorylation of DNA-PKcs, allowing phosphorylated DNA-PKcs to phosphorylate topoI and promote topoI degradation. After treatment with Rabeprazole, the HCT116 cell line shows less topoI and appears more similar to the resistant cell line HCT15. These results show the function of the phosphatase CTDSP1 as a regulator of DNA-PKcs phosphorylation may be a distinguishing factor between resistant and sensitive cell lines to CPT. Additionally, in the 0μM Rabeprazole treatment condition, cell line HCT116 does produce a dark topoI band and may be vulnerable to treatment with CPT.

TopoI levels in cell line HCT116

In order to determine whether the influence of Rabeprazole on topoisomerase levels in HCT116 cells was magnified by treatment with CPT, we conducted a western blot solely examining the sensitive cell line. When treated with 0μM and 5μM concentrations of Rabeprazole and no CPT, the darkest topoI band was produced with no inhibition of CTDSP1 in the 0μM Rabeprazole condition. The topoI band produced is characteristic of normal HCT116 cells not observed in HCT15 cells. After treatment with a 5μM concentration of Rabeprazole, HCT116 cells produced a fainter topoI band more characteristic of a resistant cell line. The decreased topoI present in the 5μM Rabeprazole condition provides evidence that CTDPS1 is a negative regulator of the topoI degradation pathway.

The latter two wells in the Figure 14 western blot detected the presence of topoI in HCT116 cells treated with CPT exposed to 0μM and 5μM Rabeprazole concentrations respectively. Both topoI bands were fainter than bands produced by HCT116 cells only exposed to different Rabeprazole conditions without CPT treatment. These results further support CPT initiates its own resistance pathway by stimulating degradation of its substrate. We expected the faintest band to be seen in the CPT treated 5μM Rabeprazole condition due to greater CTDSP1 inhibition like we observed in Figure 13. However, there was no observable difference between the topoisomerase bands made by CPT treated cells exposed to 0μM and 5μM Rabeprazole concentrations. This may be due to enhanced DNA concentration in the 5μM Rabeprazole condition, which is observed by a larger bottom band in lane 4 of Figure 14 representing actin levels as a control.

HCT 116 Cell Survival after CTDSP1 Inhibition

After looking at the effects of inhibiting CTDSP1 on both phosphorylated DNA-PKcs and topoI levels in the cell, we performed a clonogenic assay on cell line HCT116 exposed to both 0μM and 10μM Rabeprazole conditions. Each HCT116 test group was treated with 0, 0.5, 1, 2.5, 5.0, and 7.5nM concentrations of CPT. The experiment was conducted three times for the different CPT concentrations and comparisons were made using averages of results. In the 0μM Rabeprazole HCT116 cells without CTDSP1 inhibition, the greatest survival fraction of 0.01 was observed in the 0nM CPT condition. Cell death increased with higher concentrations of CPT, with the greatest depletion occurring in the 7.5 nM CPT condition with an average survival fraction of 7.75E-05. The intended function of CPT is to destroy cells by inhibiting topoI (Ando et al. 2017).

Therefore, we expected to see sensitive cell line HCT116 experience cell death with exposure to increasing concentrations of the chemotherapy treatment. The goal of the clonogenic assay was to determine whether inhibition of CTDSP1 would lead to a greater average survival fraction of HCT116 cells after treatment with CPT. In the HCT116 cells with CTDSP1 inhibited by 10μM concentrations of Rabeprazole, the survival fraction was greater in the 0nM compared to the 7.5nM CPT treatment condition with values of 0.01 and 0.0007 respectively.

While the survival fraction of HCT116 cells incubated with both 0μM and 10μM Rabeprazole was similar when treated with 0nM CPT, the survival fraction between the cell groups differed significantly between the two groups as the concentration of CPT was increased. Figure 15 demonstrates the survival fraction of HCT116 cells treated with 10μM Rabeprazole is greater than HCT116 cells with no Rabeprazole after subjection to each concentration of CPT. The increased survival fraction of HCT116 cells after treatment with CPT indicates greater cellular resistance to CPT. This data supports the hypothesis that CTDSP1 inhibition in a sensitive cell line leads to cellular resistance to CPT. The greatest differences in survival are observed in experimental groups looking at 0.5nM and 1.0nM concentrations of CPT. At concentrations greater than 1.0nM CPT concentrations, there is still greater survival in the group experiencing CTDSP1 inhibition, but the difference is less drastic.

The clonogenic assay demonstrated that when CTDSP1 is inhibited in a sensitive cell line like HCT116, the survival fraction of cells exposed to CPT increases. Additionally, differences in cell survival were not noticeable in control conditions where

cells were not treated with CPT. Previous experiments showed CTDSP1 inhibition leads to increased DNA-PKcs phosphorylation and lower levels of topoI in HCT116 cells incubated with CPT. The results of these experiments in tandem with the differences in survival fractions obtained from the clonogenic assay corroborate stimulation of the topoI degradation pathway as the mechanism responsible for cellular resistance to CPT.

Immunofluorescent Staining of phosphorylated DNA-PKcs in cell line HCT116:

In order to visualize the differences in DNA-PKcs phosphorylation in cell line HCT116 after inhibition of CTDSP1, we examined one HCT116 cell group treated with 0μM Rabeprazole and another treated with 10μM Rabeprazole under the microscope after staining pDNA-PKcs. We tagged the primary anti pDNA-PKcs antibody with a fluorescent α-Rb secondary antibody that would stain any present phosphorylated DNA-PKcs a fluorescent green. In addition to staining pDNA-PKcs, we also used the DAPI stain as a control. Because the fluorescent blue DAPI stain targets A-T regions of DNA, we expected all cells to show up as blue under the microscope. The purpose of the DAPI stain was to provide information about the amount of cells present in each slide view.

The HCT116 cell line treated with 0μM Rabeprazole revealed only a small speck of green fluorescence under the microscope despite the many cells present in the frame confirmed by the blue fluorescent DAPI stain. Minimal green fluorescence revealed there was little DNA-PKcs phosphorylation in cells without CTDSP1 inhibition. The HCT116 cell line treated with 10μM Rabeprazole showed a much greater amount of green fluorescence in comparison to the 0μM Rabeprazole experimental condition. The DAPI stain used in Figures 17 and 18 established a similar amount of cells were present in both

the 0 and 10μM Rabeprazole experimental frames. This eliminated cell number as a confounding factor and differences in DNA-PKcs phosphorylation were attributed to the difference in Rabeprazole concentration. Exposure to the larger 10μM amount of Rabeprazole led to a greater amount of DNA-PKcs phosphorylation in cells. The greater DNA-PKcs phosphorylation appears to be a significant difference between CPT resistant and sensitive cell lines that influence cellular levels of topoI. This experiment focused on imaging the HCT116 cells, but in the future it would be interesting to determine whether Rabeprazole treated HCT116 cells produced results similar to normal HCT15 imaged cells.

EGFP imaging of topoI in cell line HCT116:

Greater DNA-PKcs phosphorylation after Rabeprazole treatment determined in the previous immunofluorescent staining experiment led us to investigate the next stage of the topoI degradation pathway and examine levels of topoI after Rabeprazole treatment. We tagged fluorescent EGFP to topoI in order to visualize the difference in topoI levels in HCT116 cells after CTDSP1 inhibition. After treating cells with 0μM, 5μM, and 10μM doses of Rabeprazole, we evaluated the amount of fluorescence in each condition in comparison to the image produced by the control DAPI stain. While the results from the DAPI stain were consistent in each Rabeprazole condition, we observed the lower levels of green fluorescence in the 10μM Rabeprazole condition and a greater amount of green fluorescence in the 0μM Rabeprazole condition. Because the degree of EGFP fluorescence observed are linked to levels of topoI, these results show as CTDSP1 inhibition increases, topoI levels decline; supporting the role of CTDSP1 in the

topoisomerase degradation pathway. When the functioning of CTDSP1 was limited, more topoI was degraded. As a topoI inhibitor, CPT needs to interact with topoI in order to disrupt cellular replication and cause cell death. When less topoI is present in the cell, CPT has less substrate to interact with and is unable to effectively destroy cells. By treating HCT116 cells with the CTDSP1 inhibitor, the once CPT sensitive cell line may become more resistant to CPT. In the future, it may be beneficial to evaluate basal topoI levels in comparison to typically CPT sensitive strains in order to determine whether or not the chemotherapy treatment will be effective. If an individual's cells exhibit lower levels of topoI in comparison to the sensitive cell line, an alternative chemotherapy treatment would be recommended, sparing the patient from undergoing a painful yet ineffective round of chemotherapy treatment.

CTDSP1 Knockdown

The previous experiments produced data suggesting both CTDSP1inhibition and SN-38 treatment enhances topoI degradation. Experiments using Rabeprazole showed faster topoI degradation conferred greater cellular resistance to SN38. The next set of experiments were focused on cell line HCT116 and the HCT116 derivative cell line 12-G10. Previously the most prominent differences were observed in these sensitive cell lines, so we used these cell lines to examine the effects of CTDSP1 knockdown on cellular resistance. The same western blots produced for inhibitor experiments were performed for CTDSP1 knockdown experiments.

DNA-PKcs phosphorylation in cell lines HCT116 and 12-G10:

First, we used a western blot to detect differences in DNA-PKcs phosphorylation between cells with and without CTDSP1 knocked down in both cell lines HCT116 and 12-G10. As discussed earlier, cells without the functional CTDSP1 phosphatase would be expected to have greater DNA-PKcs phosphorylation. Previously, we noticed SN-38 treatment intensified the effects of CTDSP1 knockdown, so we incubated a set of cells in both control and knock down conditions with SN-38 for one hour. In Figure 21 we noticed darker bands in the CTDSP1 knockdown condition for HCT116 cells relative to the controls, suggesting greater DNA-PKcs phosphorylation in the absence of CTDSP1. The complete absence of a band in the HCT116 control condition without SN-38 incubation revealed that SN-38 also influences DNA-PKcs phosphorylation. In contrast, when HCT116 control cells were treated with SN-38, a faint band was produced. Even without CTDSP1 knockdown. SN-38 appeared to influence the DNA-PKcs phosphorylation in cell line HCT-116, once again suggesting that cellular resistance to CPT depends on both treatment with the drug and CTDSP1 functionality. Additionally, cell line 12-G10 showed differences between CTDSP1 knockdown and control conditions. CTDSP1 knockdown cells that were not exposed to CPT produced the darkest band, or greatest amount of phosphorylated DNA-PKcs. We expected CTDSP1 knockdown cells to produce darker bands than control cells, for we saw similar results in with greater CTDSP1 inhibition. However, we were surprised that the CTDSP1 knockdown cells incubated with CPT produced a fainter pDNA-PKcs band than the CTDSP1 knockdown cells without CPT. DNA-PKcs phosphorylation is an early step in the topoI degradation pathway and previous data suggested SN-38 enhanced the

degradation pathway of topoI. However, we also noticed the majority of bands in this lane look lighter compared to the other bands on the blot. This suggests there is less protein present overall in this lane and may explain the discrepancy.

In order to determine whether or not an error had been made with protein concentrations in the first western blot, we produced the pDNA-PKcs western blot shown in Figure 22. This time the darkest band for both HCT116 and 12-G10 cells was produced in the CTDSP1 knockdown and CPT treated condition. Additionally, even control conditions showed darker bands after CPT exposure. Greater phosphorylation of DNA-PKcs occurs when CTDSP1 is knocked down and cells are treated with CPT. These results are consistent with immunofluorescent findings in Figure 27 that show CTDSP1-knockdown cells demonstrate greater pDNA-PKcs phosphorylation, especially when treated with SN-38 compared to control cells. The differences between CTDSP1 knockdown cells incubated with and without CPT is much more drastic than the difference between control cells with and without CPT exposure. This suggests that CPT may contribute to greater DNA-PKcs phosphorylation by interfering with CTDSP1 functionality.

TopoI levels in cell lines HCT116 and 12-G10:

We continued to explore the impact of CTDSP1 knockdown and CPT treatment on the topoI degradation pathway by looking at levels of topoI in HCT116 and 12-G10 cell lines. No significant difference was observed in HCT116 cells. However, 12-G10 cells did demonstrate differences between the experimental conditions. We expected CTDSP1 knockdown cells treated with CPT to produce the faintest topoI band, revealing

accelerated degradation that would later translate to greater cellular resistance to CPT. The topoI western blot shown in Figure 23 showed the faintest band was produced in the CTDSP1 knockdown CPT treated condition. Additionally, we observed a larger actin band in the CTDSP1 knockdown CPT treated condition. Since actin was used as a control to establish constant protein concentrations, this suggests a greater amount of protein was present in this condition. Therefore, if a protein concentration more similar to the other lanes were used, the differences may be even more significant that already observed.

Because of the inconclusive results produced by cell line HCT116 in the previous experiment, we repeated the topoI western blot shown in Figure 25 using only HCT116 cell line to determine whether or not CTDSP1 knockdown had any influence on topoI degradation of these cells. This time, there was a clear difference between cells CTDSP1 knock down and control conditions. Cells with CTDSP1 knocked down produced much lighter topoI bands than cells with normal CTDSP1. Lighter bands demonstrated greater topoI degradation. Cells treated with CPT also showed fainter bands than cells in the same condition without CPT treatment. These results contribute more evidence that CTDSP1 functionality and CPT play a role in cellular resistance to CPT by enhancing topoI degradation.

Confirmation of CTDSP1 knock down in HCT116 and 12-G10 cell lines:

The results produced in the CTDSP1 knockdown experiments mirror those found in the Rabeprazole inhibition experiments. Greater CTDSP1 inhibition, as well as knockdown of CTDSP1, both lead to greater DNA-PKcs phosphorylation and topoI degradation. The effects of both knockdown and inhibition are also magnified by

exposure of cells to CPT. To confirm that the knockdown experiments were truly indicative of cells without functional CTDSP1, we produced the western blot shown in Figure 24. We used a CTDSP1 detecting antibody to determine whether CTDSP1 was present in any of the experimental conditions for both cell lines HCT116 and 12-G10. The production of large dark bands would indicate the presence of CTDSP1. The results revealed four prominent dark bands and the presence of CTDSP1 in the control conditions for both HCT1116 and 12-G10 cells. The faint bands in the CTDSP1 knockdown conditions show knockdown of CTDSP1 did occur. Because CTDSP1 was successfully knocked down, we confirmed the data produced accurately portrays the experimental conditions indicated.

Limitations

Although findings from each experiment were suggestive of the role of CTDSP1 inhibition in greater topoI degradation, there were limitations to the study. The maximum concentration of Rabeprazole used in any experiment was the small amount of 10μM. We refrained from using larger doses of Rabeprazole in order to prevent cells from dying. If cells died after treatment, we would be unable to observe differences in amounts of phosphorylated DNA-PKcs or topoI. Our experiments are limited to providing information about the impact of very small concentrations of Rabeprazole on CPT resistance.

Additionally, prior literature discusses inhibition of SCP1 family proteins as one of the functions of Rabeprazole. However, Rabeprazole is also documented as a proton pump inhibitor used for ulcer treatments (Gu et al. 2014). Currently, there are not many

literature investigations of the function of Rabeprazole. It is possible that in addition to CDTSP1 inhibition, there are other unknown functions of Rabeprazole that may influence the results of these experiments.

In the first series of experiments, we used western blots to evaluate the values of phosphorylated DNA-PKcs and topoI in cells treated with and without CPT and various concentrations of Rabeprazole. 1-hour treatment with 2.5μM CPT remained consistent for each experimental condition. The western blot results only represent cellular conditions after the 1-hour exposure to CPT. Perhaps longer treatment with CPT would make differences observed between the Rabeprazole exposed cell lines moot and ultimately destroy all the cells regardless of the amount of functioning CTDSP1.

Another caveat of using western blots involves the difficulty of producing a blot with limited interference. The topoI detecting blots produced very clear results, but the pDNA-PKcs blots were more difficult to read. Identifying the phosphorylated DNA-PKcs moiety was more challenging since phosphorylation of many proteins occurs throughout the cell. In order to produce a clearer blot, we washed the blot with buffers free of phosphate and lengthened the wash period before producing images. We also found the Immobilon-P Transfer membrane produced the most distinct pDNA-PKcs western blot image.

Producing a distinctive blot is not the only challenge of using a western blot to gather information. The validity of results depends on the knowledge that the same amount of protein was added to each well being compared. For the western blots examining topoI, we also used an anti β-actin antibody to confirm that DNA

concentrations were similar between each condition. Because the western blots examining phosphorylated DNA-PKcs already presented a lot of interference from other phosphorylated compounds, we did not use the β-actin control primary antibody. Therefore, when running the experiments, both types of western blots were conducted using the same concentrations of cell protein, so the β-actin antibody presentation on the topoI blot could be used vicariously for the pDNA-PKcs blot to indicate whether concentrations used were equivalent. To further ensure that results were accurate, we performed each experiment numerous times to ensure consistent data was being produced.

Similar to the western blot experiments, the clonogenic assay experiment was conducted using small concentrations of both CPT and Rabeprazole. Differences in pDNA-PKcs and topoI were observed with the small CPT and Rabeprazole concentrations in our experiments. Therefore, we think if concentrations of both substances were increased, then even greater differences would be observable. However, since we did not perform experiments with increased concentrations ourselves, the scope of how representative the data produced is of cellular resistance to CPT is limited.

The immunofluorescent staining of phosphorylated DNA-PKcs was also conducted carefully in order to avoid confounding results. Images under the microscope were taken immediately after the 4-hour treatment with Rabeprazole in order to capture the most accurate picture of phosphorylated DNA-PKcs. The next step in the topoI degradation pathway is phosphorylation of topoI by phosphorylated DNA-PKcs. We attempted to capture an image of phosphorylated topoI as well in this immunofluorescent

imaging experiment, but we were unsuccessful. The topoI spends a limited time in the phosphorylated state before successive degradation. Most topoI had been degraded by the time we captured an image. In order to gain more information about the amount of topoI levels in the cell, we used the EGFP read out experiment as an alternative.

Both the EGFP read out experiment and immunofluorescent phosphorylated DNA-PKcs experiment were only conducted on the sensitive cell line HCT116. We also only looked at cell line HCT116 exposed to different concentrations of Rabeprazole and neglected to treat the cells with CPT. We still do not know whether adding CPT in tandem with varying Rabeprazole concentrations as an additional variable would show more drastic results. Lastly, no imaging was conducted on the resistant HCT15 cell line, so we did not provide visual data allowing the two cell lines to be directly compared.

Future Experiments

In the future, it would be interesting to see the effects of larger concentrations of Rabeprazole on the resistance of both cell lines HCT116 and HCT15 to CPT. Further comparisons between HCT116 and HCT15 cell lines would also be helpful in determining resistant cellular characteristics. In addition to evaluating the cellular levels of pDNA-PKcs and topoI, perhaps there are additional morphological differences between the sensitive and resistant cell lines. Whether these differences may be able to be induced in the sensitive cell line HCT116 would give greater insight to the topoI degradation pathway. In addition to comparing cell lines, it would be beneficial to compare the CPT resistance of cells with PTEN and CTDSP1 knockdown. Perhaps one phosphatase has a greater influence on the topoI pathway than the other, or both

phosphatases have a similar effect. To build upon this investigation, it would be interesting to see if cellular resistance to CPT was magnified by the knockdown of both CTDSP1 and PTEN by conducting the same western blot experiments. Lastly, it would be fascinating to work with the HCT15 cell line in order to determine whether cellular resistance to CPT is reversible. The ability to both induce and remove cellular resistance to CPT via manipulation of the topoI degradation pathway will provide useful information for future chemotherapy drug design.

Applications

Understanding the effects of CTDSP1 on the topoI degradation pathway and cellular resistance to CPT can be utilized to benefit the patient community plagued by colorectal cancer. These experiments have identified high levels of DNA-PKcs phosphorylation and low levels of topoI as indicators of cellular resistance to CPT. Our research revealed these conditions are augmented by non-functional or inhibited CTDSP1, and previous studies have indicated PTEN as a phosphatase that produces results analogous to CTDSP1 (Lin et al. 2014). Conditions for these factors can be measured in sensitive cell lines to use as a baseline for comparison in a clinical setting. When consulting new patients with colorectal cancer, physicians can first take a colorectal cancer cell sample and measure basal DNA-PKcs phosphorylation levels within the cell, in addition to phosphorylated topoI and topoI. If levels of phosphorylated substrates are high, or if the amount of topoI is low, then there is a high likelihood of CTP resistance and an Oxialiplatin based treatment should be used instead.

The next step in this line of research is to determine ways to quantify the amount of these substrates to make them effective biomarkers. Developing specific antibodies for these substrates with a fluorescent tag is one avenue that can be explored in the future. In addition to pDNA-PKcs and topoI, researchers may be able to examine the functionality of CTDSP1 and PTEN in new patients. Limited activation of these phosphatases also suggests a patient will be resistant to CPT treatment.

This research takes a positive step in the direction towards personalized medicine. Rather than take a chance by putting a patient on a chemotherapy that works better for most people, doctors will have the tools to find the best treatment for a specific person. A biomarker will give physicians an opportunity to provide a patient with a better alternative treatment if there is evidence an individual's response may deviate from the majority. The successful development of a biomarker for colorectal cancer chemotherapy treatments may inspire researchers to investigate resistance trends of chemotherapy treatments for other cancers. Better understanding of drug effects and resistance patterns on different types of people will reduce the amount of issued unsuccessful chemotherapy treatments. Ultimately, this line of research has the potential to identify patients that will be responsive to medications, so chemotherapy treatments can be catered towards patient-specific needs.

APPENDIX

Table 1: Dishes of cell lines HCT15 and HCT116 exposed to varying concentrations of Rabeprazole

0μM Rabeprazole	5μM Rabeprazole	10μM Rabeprazole
Dish 1: HCT15 4E7	Dish 2: HCT15 4E7	Dish 3: HCT 15 4E7
Dish 4: HCT116 1-2 G10	Dish 5: HCT116 1-2 G10	Dish 6: HCT116 1-2 G10

Table 2: Cell Lysate Buffer Contents

Concentration	Substance
150 mM	NaCl
50 mM	Tris, pH 7.5
1%	NP-40
1 mM	DTT
1 mM	EDTA
	NaF
	NaV
	PMSF
	Pepstatin
	Aprotinin

Table 3:**Cell Lysate Buffer Contents Adjusted to be used in 10 mL volume**

Concentration	Substance	Amount (µL)
5 M	NaCl	300
1 M	Tris, pH 7.5	500
100%	NP-40	100
1 M	DTT	10
0.5 M	EDTA	20
	NaF	50
	NaV	50
	PMSF	50
	Pepstatin	50
	Aprotinin	50
	MilliQ water	8,820

Table 4: **Cell Lysate Preparation of HCT15 and HCT116 cell lines incubated with SN38 and various Rabeprazole concentrations**

Tube 1	Tube 2	Tube 3	Tube 4	Tube 5	Tube 6	Tube 7
Lysate	4E57 HCT15 + SN-38	4E57 HCT15 + SN-38	4E57 HCT15 + SN-38	12-G10 HCT116 +SN-38	12-G10 HCT116 + SN-38	12-G10 HCT116 SN-38

	0μM Rabepraz ole	5μM Rabeprazol e	10μM Rabeprazol e	0μMRabep razole	5μM Rabepraz ole	10μMRabe prazole

Table 5: Materials used to create 5% gel

	Separating	**Stacking**
Water	5.73mL	3mL
Monomer (brown bottle in the fridge) 305 acrylamide	1.67mL	660μL
Running buffer and SDS	2.6mL	650 and then 700μL
APS (10% test tube in fridge)	0.070mL or 70μL	0.070mL or 70μL
TEMED (Use immediately after adding)	7μL or 0.007mL	12μL

Table 6: Materials used to create a 7.5 percent gel

	Separating	**Stacking**
Water	4.9mL	3mL
Monomer (brown bottle in the fridge) 305 acrylamide	2.5mL	660μL
Running buffer and SDS	2.6mL	650 and then 700μL
APS (10% test tube in fridge)	0.070mL or 70μL	0.070mL or 70μL
TEMED (Use immediately after adding)	7μL or 0.007 mL	12μL

Table 7: Quantity of Sample and Marker added to each Well of the Western Blot gel

Well	**Quantity (μL)**	**Substance**
1	5	Marker
2	20	Sample
3	20	Sample
4	20	Sample

5	20	Sample
6	20	Sample
7	20	Sample
8	5	Marker

Table 8: 10cm plates of HCT116-1-2G10 cells cultured in different Rabeprazole and SN38 Conditions

Plate 1	0μM Rabeprazole	Control
Plate 2	10μM Rabeprazole	Control
Plate 3	0μM Rabeprazole	+SN-38
Plate 4	10μM Rabeprazole	+SN3-8

Table 9: Contents of the HCT116-1-2G10 6-well plate control with 0μM Rabeprazole

0nM SN-38 Added 2mL of RPMI with no SN-38	0.5nM SN-38 Added 2mL of a solution of 10mL of RPMI with 0.5μL SN-38	1.0nM SN-38 Added 2mL of a solution of 4mL of RPMI with 0.4μL SN-38
2.5nM SN-38 Added 2mL of a solution of 4mL of RPMI with 1 μL SN-38	5.0nM SN-38 Added 2mL of a solution of 4mL of RPMI with 2 μL SN-38	7.5 nM SN-38 Added 2mL of a solution of 4mL of RPMI with 3μL SN-38

Table 10: Contents of the HCT116-1-2G10 6-well plate with 10μM Rabeprazole

0 nMSN-38 Added 2mL of RPMI with 20 μL Rabeprazole with no SN38	0.5nM SN-38 Added 2mL of a solution of 10mL of RPMI with 80 μL Rabeprazole with 0.5μL SN38	1.0nM SN-38 Added 2mL of a solution of 4mL of RPMI with 20μL Rabeprazole with 0.4μL SN38
2.5nM SN-38	5.0nM SN-38	7.5nM SN-38

Added 2mL of a solution of 4mL of RPMI with 20µL Rabeprazole with 1µL SN38	Added 2mL of a solution of 4mL of RPMI with 20µL Rabeprazole with 2µL SN38	Added 7.5 nM SN38 2mL of a solution of 4mL of RPMI with 20µL Rabeprazole with 3µL SN38

Cell counting data

Table 11: Number of Cells in the 0µM Rabeprazole Control Tubes

Box	C0	C.5	C1	C 2.5	C 5	C 7.5
A	22	12	11	29	18	6
B	12	17	17	26	10	6
C	12	17	6	17	6	0
D	13	11	11	30	5	14
Average	12.25	14.25	11.25	25.5	9.75	6.5

Table 12: Number of Cells in the 10µM Rabeprazole Tubes

	R0	R 0.5	R1	R 2.5	R 5	R 7.5
A	3	13	5	6	8	5
B	0	7	0	15	8	1
C	0	12	0	11	4	5
D	0	17	2	11	0	4
Average	0.75	12.25	1.75	10.75	5.0	3.5

Table 13: CONTROL: Amount of HCT116 cells in 6 well dishes treated with 0µM Rabeprazole

Dish 1

0nM SN-38 Cell amount per/mL:1 RPMI: 121.5µL	0nM SN-38 Cell amount per/mL:1 RPMI: 121.5µL	0nM SN-38 Cell amount per/mL:1 RPMI: 121.5µL
0.5nM SN-38 Cell amount per/mL:1 RPMI: 141.5µL	0.5nM SN-38 Cell amount per/mL:1 RPMI: 141.5µL	0.5nM SN-38 Cell amount per/mL:1 RPMI: 141.5µL

Dish 2

1nM SN-38 Cell amount per/mL:1	1nM SN-38 Cell amount per/mL:1	1nM SN-38 Cell amount per/mL:1

RPMI: 111.5µL	RPMI: 111.5µL	RPMI: 111.5µL
2.5nM SN-38 Cell amount per/mL:1 RPMI: 254µL	2.5nM SN-38 Cell amount per/mL:1 RPMI: 254µL	2.5nM SN-38 Cell amount per/mL:1 RPMI: 254µL

Dish 3

5nM SN-38 Cell amount per/mL:1 RPMI: 96.5µL	5nM SN-38 Cell amount per/mL:1 RPMI: 96.5µL	5nM SN-38 Cell amount per/mL:1 RPMI: 96.5µL
7.5nM SN-38 Cell amount per/mL:1 RPMI: 65µL	7.5nM SN-38 Cell amount per/mL:1 RPMI: 65µL	7.5nM SN-38 Cell amount per/mL:1 RPMI: 65µL

Table 14: Amount of HCT116 cells in 6-well dishes treated with 10µM Rabeprazole

Dish 4

0nM SN-38 Cell amount per/mL:4 RPMI: 26µL	0nM SN-38 Cell amount per/mL:4 RPMI: 26µL	0nM SN-38 Cell amount per/mL:4 RPMI: 26µL
0.5nM SN-38 Cell amount per/mL:1 RPMI: 121.5µL	0.5nM SN-38 Cell amount per/mL:1 RPMI: 121.5µL	0.5nM SN-38 Cell amount per/mL:1 RPMI: 121.5µL

Dish 5

1nM SN-38 Cell amount per/mL:1 RPMI: 16.5µL	1nM SN-38 Cell amount per/mL:1 RPMI: 16.5µL	1nM SN-38 Cell amount per/mL:1 RPMI: 16.5µL
2.5nM SN-38 Cell amount per/mL:1 RPMI: 196.5µL	2.5nM SN-38 Cell amount per/mL:1 RPMI: 106.5µL	2.5nM SN-38 Cell amount per/mL:1 RPMI: 106.5µL

Dish 6

5nM SN-38 Cell amount per/mL:1 RPMI: 49µL	5nM SN-38 Cell amount per/mL:1 RPMI: 49µL	5nM SN-38 Cell amount per/mL:1 RPMI: 49µL
7.5nM SN-38 Cell amount per/mL:1 RPMI: 34µL	7.5nM SN-38 Cell amount per/mL:1 RPMI: 34µL	7.5nM SN-38 Cell amount per/mL:1 RPMI: 34µL

Table 15: **6-well dish contents of HCT116 cells exposed to 0µM and 10µM Rabeprazole Conditions**

Control HCT116 cells 0µM Rabeprazole	Control HCT116 cells 0µM Rabeprazole	Empty
HCT 116 cells 10µM Rabeprazole	HCT116 cells 10µM Rabeprazole	Empty

Table 16: siRNA Resuspension Volumes and Concentrations

siRNA Amount (nmol)	1xsiRNA Buffer to be added (µL) for desired final concentration **100µM Stock**	1xsiRNA Buffer to be added (µL) for desired final concentration **20µM Stock**
5.0	50	250

Table 17: Cell line HCT116 6-well Dish

Control +SN-38	siRNA +SN-38	Empty
Control	siRNA	Empty

Table 18: Cell line 12-G10 6-well Dish

Control +SN-38	siRNA +SN-38	Empty
Control	siRNA	Empty

Table 19: Cell Lysate Preparation of HCT116 and 12-G10 cell lines with and without functional CTDSP1

Tube 1	Tube 2	Tube 3	Tube 4	Tube 5	Tube 6	Tube 7	Tube 8
HCT116 control -SN-38	HCT116 control +SN-38	HCT116 +siRNA -SN-38	HCT116 +siRNA +SN-38	12-G10 control -SN-38	12-G10 control +SN-38	12-G10 +siRNA -SN-38	12-G10 +siRNA +SN-38

Table 20: Materials used to create 10% gel

	Separating	**Stacking**
Water	5.73mL	3mL
Monomer (brown bottle in	1.67mL	660µL

the fridge) 305 acrylamide		
Running buffer and SDS	2.6mL	650 and then 700µL
APS (10% test tube in fridge)	0.070mL or 70µL	0.070mL or 70µL
TEMED (Use immediately after adding)	7µL or 0.007mL	12µL

LIST OF JOURNAL ABBREVIATIONS

ASPET	The American Society for Pharmacology and Experimental Therapeutics
	Cancer Research
GANN	Japanese Journal of Cancer Research
MCT	Molecular Cancer Therapeutics
	Molecular Pharmacology
NG	Nature Genetics

REFERENCES

Ando, Koji, Ankur Shah, Vibhu Sachdev, Benjamin Kleinstiver, and Julian Taylor-Parker. "Camptothecin Resistance Is Determined by the Regulation of Topoisomerase I Degradation Mediated by Ubiquitin Proteasome Pathway." *Oncotarget* (2017): n. pag. Web.

Arakawa, Y., H. Suzuki, S. Saito, and H. Yamada, Novel missense mutation of the DNA topoI gene in SN-38 resistant DLD-1 Cells. Molecular cancer therapeutics, 2006. 5(3): p. 502-8

Desai, S.D., Li, T.K., Rodriguez-Bauman, A., Rubin, E.H., and Liu, L.F. (2001). Ubiquitin/26S proteasome-mediated degradation of topoI as a resistance mechanism to CPTptothecin in tumor cells. Cancer Research 61, 5926-5932.

Fujimori, Akira, Malini Gupta, Yuko Hoki, and Yves Pommier. "Acquired CPTptothecin Resistance of Human Breast Cancer MCF-7/C4 Cells with Normal TopoI and Elevated DNA Repair." *The American Society for Pharmacology and Experimental Therapeutics* (1996): 1473-478. Print.

Goldwasser, F., Bae, I., Valenti, M., Torres, K., and Pommier, Y. TopoI-related parameters and CPT activity in the colon carcinoma cell lines from the National Cancer Institute Anticancer screen. Cancer Research *55:* 2116–2121, 1995.

Gu, Mengli et al. “Rabeprazole Exhibits Antiproliferative Effects on Human Gastric Cancer Cell Lines.” *Oncology Letters*, D.A. Spandidos, Oct. 2014,

www.ncbi.nlm.nih.gov/pmc/articles/PMC4156221/.

Hsiang YH, Liu LF. Identification of mammalian DNA topoisomerase I as an intracellular target of the anticancer drug camptothecin. Cancer research 1988;48(7):1722-6.

Kashuba VI, Li J, Wang F, Senchenko VN, Protopopov A, Malyukova A, et al. RBSP3 (HYA22) is a tumor suppressor gene implicated in major epithelial malignancies. Proceedings of the National Academy of Sciences U S A 2004;101: 4906–4911

Lee, J.S., Paull, K., Alvarez, M., Hose, C., Monks, A., Grever, M., Fojo, A.T., and Bates, S.E. (1994). Rhodamine efflux patterns predict P-glycoprotein substrates in the National Cancer Institute drug screen. Molecular Pharmacology *46*, 627–638.

Lin, Y.-C. et al. "SCP Phosphatases Suppress Renal Cell Carcinoma by Stabilizing PML and Inhibiting MTOR/HIF Signaling." *Cancer Research*, vol. 74, no. 23, July 2014, pp. 6935–6946. doi:10.1158/0008-5472.can-14-1330.

Liu LF, Desai SD, Li TK, Mao Y, Sun M, Sim SP. Mechanism of action of camptothecin. Annals of the New York Academy of Sciences **2000**;922:1-10.

Molecular Pathology Unit, Center for Cancer Research, and Center for Computational and Integrative Biology, Massachusetts General Hospital, Charlestown, Massachusetts 02129, USA.

Nesti, Edmund et al. "C-Terminal Domain Small Phosphatase 1 and MAP Kinase Reciprocally Control REST Stability and Neuronal Differentiation." *Proceedings*

of the National Academy of Sciences of the U S A, vol. 111, no. 37, Feb. 2014, doi:10.1073/pnas.1414770111.

Ohashi, N., Y. Fujiwara, N. Yamaoka, O. katoh, Y. Satow, and M. Yamakido, No alteration in DNA topoI gene related to CPT-11 resistance in human lung cancer. Japanese journal of cancer research: Gann, 1996. 87 (12): p. 1280-7.

Potmesil, M., CPTptothecins: from bench research to hospital wards. Cancer research, 1994. 54(6): p. 1431-9.

Scherf, U., D.T. Ross, M. Waltham, L.H, Smith, J,K, Lee, L, Tanabe, K.W. Kohn, W.C. Reinhold, T.G. Myers, D.T. Andrews, D.A. Scudiero, M.B. Eisen, E.A. Sausville, Y. Pommier, D. Bostein, P.O. Brown, and J.N. Winstine A gene expression database for the molecular pharmacology of cancer. Nature genetics, 2000. 24(3): p. 236-44.

Szakacs, G., J,P, Annereau, S. Lababidi, U. Shankarvaram, A. Arciello, K.J. Bussey, W. Reinhold, Y. Guo, G.D. Kruh, M. Reimers, J.N. Weinstein, and M.M. Gottesman, Predicting drug sensitivity and resistance: profiling ABC transporter genes in cancer cells. Cancer cell, 2004. 6(2):p. 129-37.

Wang, W et al. "SCP1 Regulates c-Myc Stability and Functions through Dephosphorylating c-Myc Ser62." *Oncogene*, vol. 35, no. 4, 2015, pp. 491–500. doi:10.1038/onc.2015.106.

Wolyniec K, Shortt J, de Stanchina E, Levav-Cohen Y, Alsheich-Bartok O, Louria-Hayon I, et al. E6AP ubiquitin ligase regulates PML-induced senescence in Myc-driven lymphomagenesis. Blood 2012;120: 822–32.

Zhang, Mengmeng et al. "Selective Inactivation of a Human Neuronal Silencing Phosphatase by a Small Molecule Inhibitor." *ACS Chemical Biology*, vol. 6, no. 5, 2011, pp. 511–519. doi:10.1021/cb100357t.

CURRICULUM VITAE